UC Berkeley
UC Berkeley Electronic Theses and Dissertations

Title
Late Holocene Climate Change on Isla Isabela, Gulf of California

Permalink
https://escholarship.org/uc/item/5p38g9pj

Author
Englebrecht, Amy

Publication Date
2010

Peer reviewed|Thesis/dissertation

eScholarship.org Powered by the California Digital Library
University of California

Late Holocene Climate Change on Isla Isabela, Gulf of California

by

Amy Cathryn Englebrecht

A dissertation submitted in partial satisfaction of the

requirements for the degree of

Doctor of Philosophy

in

Earth and Planetary Science

in the

Graduate Division

of the

University of California, Berkeley

Committee in charge:

Professor B. Lynn Ingram, Chair
Professor A. Roger Byrne
Professor James Bishop

Fall 2010

Abstract

Late Holocene Climate Change on Isla Isabela, Gulf of California

by

Amy Cathryn Englebrecht

Doctor of Philosophy in Earth and Planetary Science

University of California, Berkeley

Professor B. Lynn Ingram, Chair

Sediments from the crater lake on Isla Isabela, in the southern Gulf of California, were used to investigate precipitation and evaporation changes in this region over the past 6,000 years. Stable isotopes of oxygen and carbon provided a proxy record of Pacific climate variability on timescales ranging from decadal to millennial. Strength in the dominant periodicities of the Pacific Decadal Oscillation appears to have been intermittent over the past two millennia, suggesting changes in Pacific forcing not previously recognized. In addition, productivity in the lake varies on timescales that suggests a link between increased productivity and solar maxima. Although the precise role of solar activity on climate variations remains unclear, this data represents a convergence of model output with empirical evidence over the past millennium. Over the late Holocene, it appears that there have been a number of pronounced dry periods that generally coincide with cold sea surface temperatures in the eastern Pacific, and generally dry conditions across western North America.

ACKNOWLEDGEMENTS

I owe many thanks to my mentors and coauthors: Lynn Ingram, Tom Guilderson, Roger Byrne, Jim Bishop, Harald Böhnel, Ulrike Kienel, and Gerald Haug. Dave Wahl and Liam Reidy were crucial in the initial field efforts on Isabela, and Wenbo Yang, Shaun Brown, and Paula Zermeno provided key analytical assistance.

This work was supported by a National Science Foundation Graduate Research Fellowship, a Berkeley Atmospheric Sciences Center Graduate Research Grant, and a Lawrence Livermore National Laboratory Lawrence Scholar Fellowship. Additional support was provided by the Lawrence Livermore National Laboratory Directed Research and Development Grant 09ERI003. Fieldwork was funded by the Helmholtz Centre PotsdamGFZ, and by the German Research Association DFG.

CHAPTER 1

INTRODUCTION

1.1 Introduction

Located at the northern edge of the tropics, the Gulf of California is a region of competing atmospheric, oceanographic, and geographic effects. The climate is monsoonal, with marked seasonal changes in wind direction and precipitation (Douglas et al., 1993; Adams and Comrie, 1997; Higgins et al., 1998). The region is also an area of water mass transition, between the north equatorial system and the North Pacific gyre. Two surface currents impact this region, the California Current and the Costa Rica Current, and both vary significantly through the annual cycle in response to insolation-driven changes in wind systems (Baumgartner and Christensen, 1985). The geography of the Gulf is also critical to its climate. As a deep, narrow, northwest to southeast trending sea, it is bounded by the arid Baja California peninsula to the west and the Sonoran Desert to the east. The dry surroundings constrain its evaporative continental climate, in contrast with the more temperate marine climate commonly associated with the California Current.

The North American Monsoon is characterized by strong seasonal variations in the winds, sea surface temperature (SST) and rainfall (Bordoni et al., 2004), and has basically two modes, winter (cool and dry) and summer (wet and warm). Seasonal changes in the latitudinal position and strength of the North Pacific High (NPH) pressure system, control the seasonally reversing winds along the Gulf (Badan-Dangon et al., 1991).

The winter (November to March) mode is dominated by strong northwesterly winds and lowered SSTs. The winds intensify in the fall as the NPH and the Intertropical Convergence Zone (ITCZ) retreat equatorward (Pares-Sierra et al., 2003; Bordoni et al., 2004), and the winds from the anticyclonic flow around the NPH are channeled down the axis of the Gulf by the high topography on both sides. The winter winds lower SSTs and generate upper ocean mixing and enhanced Ekman transport along the eastern margin of the Gulf (Alvarez-Borrego and Lara-Lara, 1991; Thunnell et al., 1996).

In contrast, the summer (April to October) mode introduces higher SSTs, higher humidity and rainfall. Northwesterly winds diminish as the NPH and the ITCZ shift northward, and are replaced by irregular southerly winds (Bordoni et al., 2004). These southerly winds are modulated by "Gulf surges" that originate in cyclonic disturbances over the east Pacific warm pool off Central America and propagate northward into the subtropics. In the core of the summer monsoon (June to August), a combination of high elevation (mid-troposphere) winds, convective storms and Gulf surges transport moisture-laden tropical air into the Gulf and produce 60-80% of the annual rainfall (Bordoni and Stevens, 2005), with the majority of the rain concentrated along the western flank of the Sierra Madre Occidental and extending into the U.S. desert southwest (Douglas et al., 1993). The introduction of eastern tropical Pacific surface water by the Costa Rica Current, typically beginning in April-May (Castro et al., 2000) and the northward shift of the 28°C isotherm governs this northward propagation of convective storms and rainfall (Mitchell et al., 2002). By mid-summer, a thick layer (up to 150 m) of warm (>28°C) water covers the southern and central Gulf (Bray, 1988). During this time, wind-driven upwelling is weak and limited to the western side of the Gulf (Alvarez-Borrego and Lara-Lara, 1991; Bray and Robles, 1991).

Although the annual climate cycle of the region is generally a seesaw between the two monsoon modes, the duration and relative strength of each mode varies in response to insolation forcing on several timescales, from seasonal and interannual to centennial and millennial (e.g., Douglas et al., 2002, 2007; Barron et al., 2003, 2004; Herguera et al., 2003). Modeling studies

(Liu et al., 2003; Clement et al., 1999) and the sediment record (Barron et al., 2004) both suggest that the winter mode dominated from 3-5 ky BP as the mean position of the ITCZ moved south in the late Holocene. In the earlier Holocene, seasonality was greater and the summer mode was more dominant (Douglas et al., 2007; Liu et al., 2003).

1.2 Goals of Thesis

Sediment cores from the crater lake on Isla Isabela, in the southern Gulf of California, were used to investigate precipitation and evaporation changes in this region over the past 6,000 years. These sediments represent a unique archive of climate changes in the region, providing a continuous, high-resolution record spanning several thousand years—a resolution and duration that has not been achieved in this area before. The topics addressed in the following chapters are:

Pacific Decadal Oscillation variability over the past 2,000 years (Chapter 2)

Linking solar activity and Pacific climate variability (Chapter 3)

Long-term patterns in drought recurrence (Chapter 4)

1.3 References

Adams, D.K., Comrie, A.C. 1997. The North American monsoon. Bulletin of the American Meteorological Society 78(10): 2197-2213.

Alvarez-Borrego, S., Lara-Lara, J.R. 1991. The physical environment and primary productivity of the Gulf of California. In Dauphin, J.P., Simoneit, B.R.T. (eds.) The Gulf and Peninsular Provinces of the Californias. AAPG Memoir 47: 555-568.

Badan-Dangon, A., Dorman, C.E., Merrifield, M.A., Winant, C.D. 1991. The lower atmosphere over the Gulf of California. Journal of Geophysical Research 96(C9): 16,877–16,896.

Barron, J.A., Bukrya, D., Bischoff, J.L. 2004. High resolution paleoceanography of the Guaymas Basin, Gulf of California, during the past 15 000 years. Marine Micropaleontology 50(3-4): 185-207.

Barron, J.A., Bukry, D., Bischoff, J.L. 2003. A 2000-yr-long record of climate from the Gulf of California. In West, G.J. and Blomquist, N.L. (eds.) Proceedings of the Nineteenth Pacific Climate Workshop, Asilomar, Pacific Grove, CA, March 3-6, 2002.

Baumgartner, T.R., Christensen, N. 1985. Coupling of the Gulf of California to large-scale interannual climatic variability. Marine Research 43: 825-848.

Bordoni, S., Ciesielski, P.E., Johnson, R.H., McNoldy, B.D., Stevens, B. 2004. The low-level circulation of the North American Monsoon as revealed by QuikSCAT. Geophysical Research Letters 31: L10109.

Bordoni, S., Stevens, B. 2005. Principal component analysis of the summertime winds over the Gulf of California: a gulf surge index. Monthly Weather Review 134: 3395-3414.

Bray, N.A. 1988. Thermohaline circulation in the Gulf of California. Journal of Geophysical Research 93(C5): 4993–5020.

Bray, N.A., Robles, J.M. 1991. Physical oceanography of the Gulf of California. In Dauphin, J.P., Simoneit, B.R.T. (eds.) The Gulf and Peninsular Provinces of the Californias. AAPG Memoir 47: 511-554.

Castro, C.L., McKee, T.B., Pielke, R.A. 2000. The relationship of the North American Monsoon to tropical and north Pacific sea surface temperatures as revealed by observational analyses. Journal of Climate 14: 4449-4473.

Clement, A.C., Seager, R., Cane, M.A. 1999. Suppression of El Nino during the mid-Holocene by changes in the earth's orbit. Paleoceanography 15(6): 731-737.

Douglas, M.W., Maddox, R.A., Howard, K. 1993. The Mexican Monsoon. Journal of Climate 6: 1665-1677.

Douglas, R.G., Gorsline, D., Grippo, A., Granados, I., Gonzalez-Yajimovich, O. 2002. Holocene ocean-climate variation in Alfonso Basin, Gulf of California, Mexico. In West, G.J., Buffaloe, L.D. (eds.) Proceedings of the Eighteenth PACLIM Workshop. Asilomar, Pacific Grove, CA, pp. 7-20.

Douglas, R., Gonzalez-Yajimovich, O., Ledesma-Vazquez, J., Staines-Urias, F. 2007. Climate forcing, primary production and the distribution of Holocene biogenic sediments in the Gulf of California. Quaternary Science Reviews 26: 115-129.

Herguera, J.C., Franco, G.B., Molina-Cruz, A. 2003. Decadal surface ocean variability in the lower Gulf of California: records for the past 300 years. Geofisica Internacional 42(3): 397-406.

Higgins, R.W., Mo, K.C., Yao, Y. 1998. Interannual variability of the U.S. summer precipitation regime with emphasis on the southwestern monsoon. Journal of Climate 11: 2582-2606.

Liu, Z., Otto-Bliesner, B., Kutzbach, J., Li, L., Shields, C. 2003. Coupled climate simulation of the evolution of global monsoons in the Holocene. Journal of Climate 16(15): 2472–2490.

Mitchell, D.L., Ivanova, D., Rabin, R., Brown, T.J., Redmond, K. 2002. Gulf of California sea surface temperatures and the North American monsoon: mechanistic implications from observations. Journal of Climate 15: 2261-2281.

Pares-Sierra, A., Mascarenhas, A., Marinone, S.G., Castro, R. 2003. Temporal and spatial variation of the surface winds in the Gulf of California. Geophysical Research Letters 30(6): 1312-1315.

Thunell, R., Pride, C., Tappan, E., Muller-Karger, F.E. 1996. Plankton response to physical forcing in the Gulf of California. Journal of Plankton Research 18: 2017-2026.

CHAPTER 2

VARVED RECORD OF PACIFIC DECADAL OSCILLATION VARIABILITY OVER THE PAST 2,000 YEARS

Abstract

Although the Pacific Decadal Oscillation (PDO) is commonly considered a North Pacific phenomenon, atmospheric feedbacks result in decadal precipitation and temperature variability across the Pacific Basin. But key questions remain of the past behavior of the PDO. A 2,000-year record of the PDO reconstructed from the oxygen isotope composition of a continuous varved sequence from Isla Isabela provides some answers to these questions. The PDO appears to have been in positive phase during most of the Medieval Climate Anomaly (MCA; AD 800 to 1100), and in a prolonged negative phase prior to the MCA, from about AD 550 to 750. However, strength in the dominant periodicities of the PDO appears to have been intermittent over the past two millennia, suggesting changes in Pacific forcing not previously recognized.

2.1 Introduction

The Pacific Decadal Oscillation (PDO) is a recognized aspect of ocean-atmosphere variability that impacts water resource management, fisheries management, and global climate projections (Barlow et al., 2001; Gedalof and Smith, 2001; Chavez et al., 2003; Clement et al., 2009). Positive phases of the PDO are characterized by anomalously cold sea surface temperatures (SST) in the central North Pacific and warm SST anomalies in the subtropical Northeast Pacific and along the northwestern coast of North America. Positive PDO phases have a similar dipole effect on the North American landmass, with above normal winter precipitation in the southwest United States and northwest Mexico, and below normal winter precipitation, snowpack and streamflow in the northwest United States and Canadian Great Plains. During negative phases these teleconnection patterns reverse. Alternating phases of the PDO can last for two to three decades, and the transitions from positive to negative phases (regime shifts) can have drastic effects on ecosystems and communities (Francis and Hare, 1994; Mantua et al., 1997; Finney et al., 2002).

Although the PDO was first recognized in 20th century instrumental SST data from the North Pacific (Mantua et al., 1997), the history of the phenomenon over the past several centuries has since been reconstructed from tree rings and coral records at many sites around the Pacific Basin (Linsley et al., 2000; Biondi et al., 2001; D'Arrigo et al., 2001; Gedalof et al., 2004; MacDonald and Case, 2005). These records have shown decadal changes in both temperature and precipitation associated with the PDO, but lack continuity beyond a few centuries, with the longest composite tree ring record of the PDO from western Canada and southern California dating to AD 993 (MacDonald and Case, 2005). In some cases, these time series also exhibit significant heterogeneity (Gershunov and Barnett, 1998; Gedalof et al., 2002). Key questions remain about long-term variability in the PDO as well as extrapolation between regionally restricted proxy-data records.

Here, we present a 2,000-year record from varved lake sediments from Isla Isabela, an island in the southern Gulf of California (Figure 2.1). Seasonal changes in the latitudinal position and strength of the North Pacific High control the seasonally reversing winds along the Gulf of California and lead to the formation of a strong annual cycle in SST and precipitation that basically has two modes, winter (cool and dry) and summer (wet and warm). Due to the strong annual cycle in rainfall, climate records from this region are very sensitive to changes in moisture balance (Biondi et al., 2001).

2.2 Material and methods

The core was collected from Isabela Crater Lake in December 2006. The anoxic bottom waters and high sedimentation rate (average 2 mm/y over the past 2,000 years) minimize post-depositional alteration associated with bioturbation, making the site optimal for monitoring long-term changes in moisture balance. The sediment displays alternating light and dark laminations with episodic layers of macroscopic calcium carbonate. The light laminations are composed of carbonates, organic material from algae and bacteria, ostracod shells and varying amounts of clastic material. The dark laminations are composed of organic material, principally from algae and bacteria. The macroscopic calcium carbonate is largely biogenic in origin, indicated by aragonite mineralogy and morphologies (microspheres and dumbbells) observed in thin section.

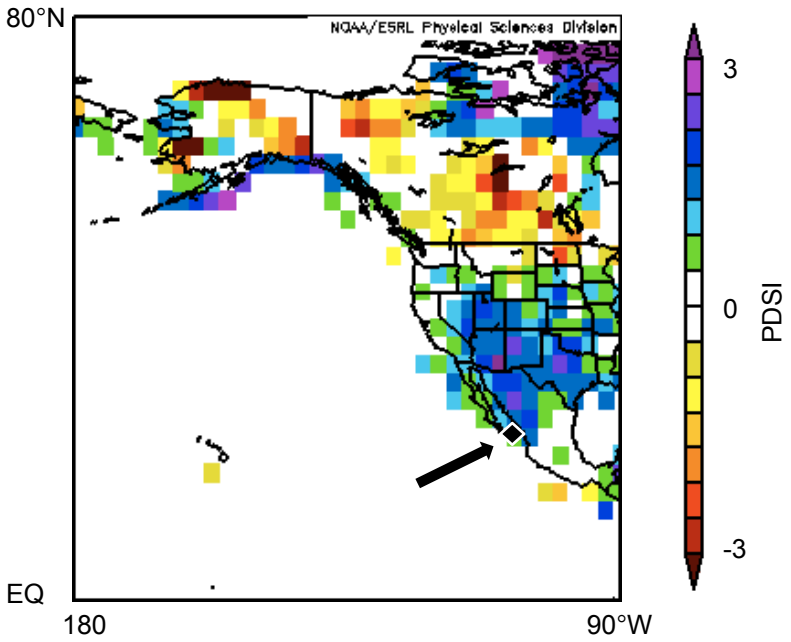


Figure 2.1. Palmer Drought Severity Index (PDSI) for winter (JFM) precipitation during a positive PDO phase (1977-1998). Cool colors (positive index) generally indicate wetter conditions and warm colors (negative index) indicate drier conditions. During the negative phase of PDO, the north-south dipole reverses, so that the southwest United States and northwest Mexico are generally drier and the northwest US and Canadian Great Plains are generally wetter. Location of study site (22°N, 106°W) is shown by black diamond. Image provided by the NOAA-ESRL Physical Sciences Division, Boulder, CO from web site at http://www.esrl.noaa.gov/psd/ (Kalnay et al., 1996).

Diatoms present in the sediments are always of the same species (*Amphora* cf. *coffeaeformis*), and alternate within the same year with cyanobacteria and heterotrophic and sulfate reducing bacteria, which occur at different water depths in the modern water column. Mean varve thickness during the past 2,000 years is 2.1 mm, and varies between ~ 1-7 mm.

A 5-m-long composite section was constructed using nine overlapping core sections. The chronology is based on varve counts supported by ten ^{210}Pb dates in the core top and six AMS-^{14}C dates downcore. For oxygen isotope ($\delta^{18}O$) analysis, sediment samples were taken at 1-3 cm intervals, averaging ~ 3-5 y of deposition. Sediments were sieved to separate the fine fraction (63-125 μm), and aliquots of sediment containing 0.1-0.5 mg carbonate were reacted with phosphoric acid to produce CO_2 (McCrea, 1950). Oxygen isotope measurements were made on a GV Instruments JB Series Isoprime mass spectrometer with a dual inlet multiprep system optimized for analysis of small carbonate samples. Oxygen isotope data are reported in the δ notation relative to the Pee Dee Belemnite (PDB) standard. The internal precision of the $\delta^{18}O$ measurements is ±0.05‰, and repeated measurements had a standard deviation of 0.5‰.

The radiocarbon ages were determined using ~1 mg samples of bulk acid insoluble organic matter. Sediment samples were acidified at 90°C using 1N HCl, rinsed with distilled water to neutral pH, and dried overnight. Following combustion to CO_2, samples were reduced to graphite using iron as a catalyst, after Vogel et al. (1984). A standard coal blank was treated simultaneously with the samples and used for background subtraction. Radiocarbon content was measured at the Center for Accelerator Mass Spectrometry (CAMS), at Lawrence Livermore National Laboratory. Radiocarbon ages are reported using the Libby half-life of 5568 yr, following standard conventions (Stuiver and Polach, 1977), and includes a $\delta^{13}C$ correction of -23‰. For calibration, a ΔR of 360 yr was applied to correct for a local pre-aged carbon effect, and calibrated ages were determined using CALIB 6.0 (Reimer et al., 2009). An age model was constructed using the ARAND software program (Howell et al., 2006). Radiocarbon dates and calibrated ages are listed in Table 2.1.

Table 2.1. Raw radiocarbon and calibrated ages of the acid insoluble fraction of bulk sediments.

CAMS #	Depth (cm)	^{14}C age (^{14}C yr BP)	±	1σ cal age range (cal BP)	2σ cal age range (cal BP)	Median probability age (cal BP)
136255	12	360	35	-	-	-
140535	78	580	35	149-186	138-223	182
140536	178	1105	35	661-693	652-730	680
140537	278	1445	35	934-987	930-1018	982
140538	280	1450	35	953-1000	932-1056	988
140539	380	2105	35	1605-1700	1549-1718	1645

2.3 Results and Discussion

The oxygen isotope ratio of carbonate in sediments is a proxy long recognized for its potential to provide high-resolution information about rapid climate changes (Talbot and Kelts, 1990; McKenzie and Hollander, 1993). In order to calibrate the hydrologic variations at this site, we compared the $\delta^{18}O$ in the core top to the observed PDO index (Figure 2.2). Shifts toward more elevated $\delta^{18}O$ correspond to negative phases of the PDO, suggesting that these periods are characterized by increased evaporation relative to precipitation at Isabela Crater Lake, and vice versa. The $\delta^{18}O$ variations generally reflect changes in moisture balance; temperature effects, which influence both the isotopic composition of the rainfall and fractionation during $CaCO_3$ precipitation, are of secondary importance in subtropical closed basin lakes, being generally masked by evaporative- and residence-related effects (Stuiver, 1970).

Over the entire record, the largest isotopic fluctuations and lowest $\delta^{18}O$ values occur AD 1250 to 1350, with a range of approximately 5‰ and a minimum value of -5‰ (Figure 2.3; Appendix A). The highest $\delta^{18}O$ values, suggesting drier conditions, occur AD 550 to 750 and 1850 to 1900. The most prominent feature of our oxygen isotope record is $\delta^{18}O$ values of -2‰ from AD 800 to 1100, suggesting wetter than average conditions during the time that is broadly coincident with the Medieval Climate Anomaly (MCA). Also, an increase in $\delta^{18}O$ values from -2 to 1‰ suggests a general drying trend from AD 1600 to 1900. These observations generally coincide with variations recorded in other proxies from around the Pacific Basin. Drier conditions in British Columbia and the Canadian subarctic AD 800-1000 (Bennett, 1999; Pienitz et al., 2000) fit the general teleconnection patterns of a positive PDO phase, with drier conditions in northwest North America and wetter conditions in northwest Mexico and southwest US (Figure 1). Other proxy records show increased productivity in the Santa Barbara basin (Kennett and Ingram, 1995) and Gulf of California (Juillet-Leclerc and Schraer, 1987) during this time period. In addition, tree ring evidence for a negative PDO from AD 1600 to 1800 (MacDonald and Case, 2005) coincides with our observation of general drying from AD 1600 to 1900.

The recurrence period of the PDO has remained a pressing question (Benson et al., 2003; MacDonald and Case, 2005). Periodicities of 15- to 25- years (Minobe, 1997) and 50- to 70-years (Minobe, 1999) have been identified for the PDO, but records have shown that the periods of variability have not been consistently present (MacDonald and Case, 2005). In order to examine the variability in the PDO periodicities, the oxygen isotope record was detrended and interpolated (15-year resolution), then subjected to wavelet analysis (Torrence and Compo, 1998). The significance of peaks in the wavelet power spectrum was tested against an autoregressive red noise background spectrum. Strength in the PDO periodicities is intermittent over the past two millennia (Figure 2.4). The greatest strength in the multidecadal PDO bands appears from AD 1100 to 1350, 1500 to 1600, and 1800 to 1900. But the strength at the PDO periodicities is largely absent outside of these time ranges. Strength in the bidecadal band from AD 1100 to 1300 corresponds to the lowest measured $\delta^{18}O$ values of the entire record, suggesting wet conditions at the conclusion of the MCA. The MCA has been previously recognized as a time of general instability, when the modes of feedbacks between ocean-atmospheric circulation and northern Pacific ecosystems appeared to have changed (Finney et al., 2002).

While the PDO is predominantly thought of as representing shifts in SST in the North Pacific, these changes are accompanied by corollary changes in wind strength and precipitation patterns as a result of feedbacks as tropical and subtropical atmospheric circulation adjusts to the

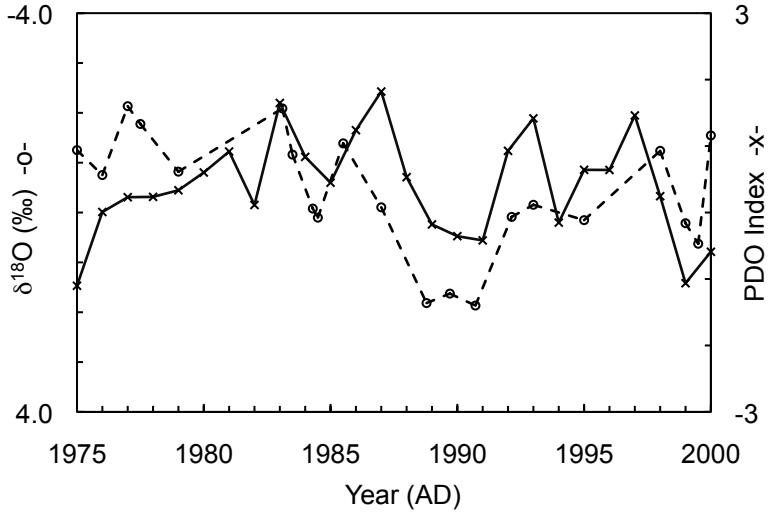


Figure 2.2. Oxygen isotopic composition ($d^{18}O$) from individual varves (circles) compared to observed annual PDO (crosses). Note reversed $d^{18}O$ scale, with wetter conditions up and drier conditions down. PDO data provided by JISAO from web site at http:// jisao.washington.edu/pdo/PDO.latest (Mantua et al., 1997).

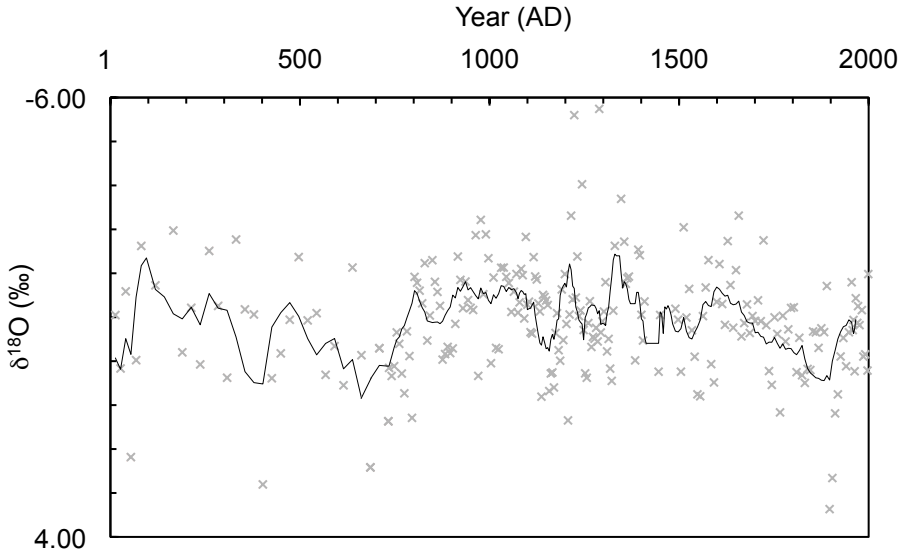


Figure 2.3. Individual measurements (crosses) and five-point running mean of sediment $\delta^{18}O$.

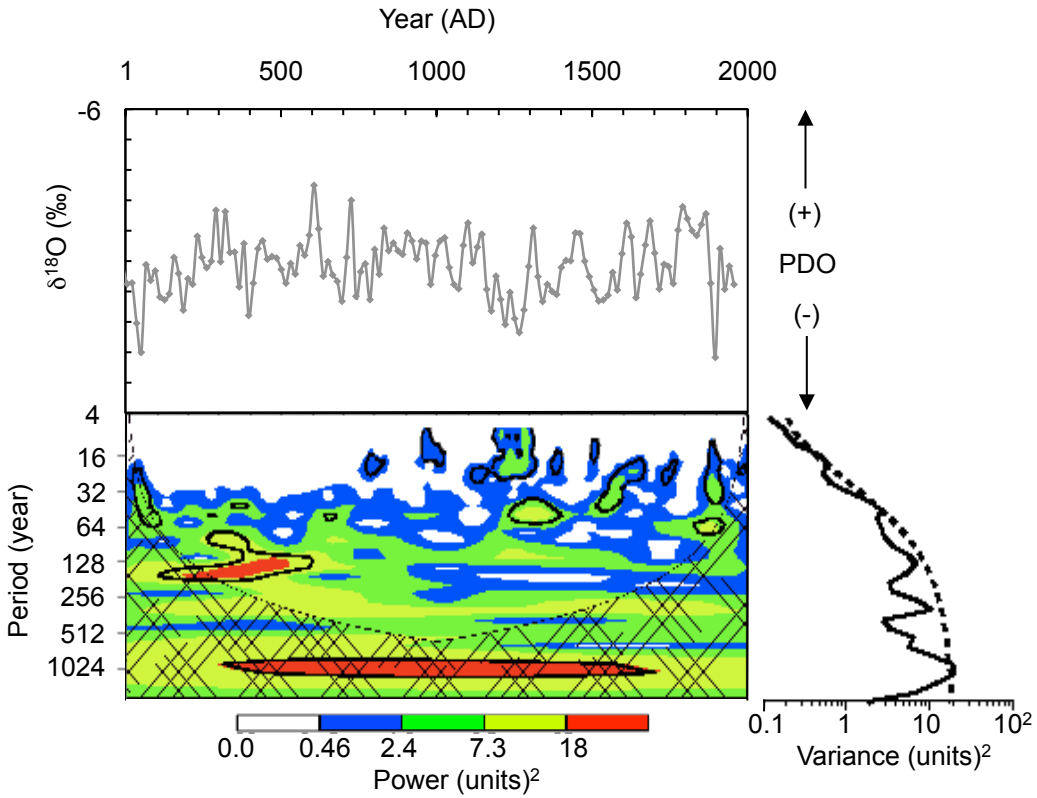


Figure 2.4. Climate records and wavelet analysis (Torrence and Compo, 1998), counterclockwise from top left: detrended and 15-yr interpolated $\delta^{18}O$; wavelength power spectrum of $\delta^{18}O$ showing significant periodicities ($p \leq 0.05$) outlined in black; global wavelet profile, with significant periodicities extending to or beyond dashed curve. Cross-hatching indicates the cone of influence, where edge effects may be important.

new pattern of heating (Hare and Mantua, 2000; MacDonald and Case, 2005; Clement et al., 2009). The pattern of the SST anomalies of the PDO has led to its description as persistent phases of ENSO (Zhang et al., 1997). While the spatial pattern is similar to that associated with ENSO (warm anomalies in the tropics and cool anomalies in the high latitudes during the warm phase, and the converse during the cool phase) the PDO exhibits lower amplitudes of SST variability in the tropics and higher amplitude outside of the tropics (Zhang et al., 1997). Recent work has shown that when SSTs are warm (cold) in the Northeast Pacific, the SLP pattern comprises a weaker (stronger) Walker circulation in the equatorial region, as well as weaker (stronger) subsidence and lower (higher) tropospheric stability in the eastern Pacific (Clement et al., 2009). But how the low frequency PDO feeds back on the higher frequency ENSO variability is not clear. Evaluation of ENSO indices and the PDO have shown a correspondence, with ENSO appearing to be modulated by the background state of the climate system and the PDO. This does not mean that the PDO physically controls ENSO, rather that the resulting climate patterns interact with each other, and the climate background state and PDO are important components of how ENSO is expressed.

High-resolution paleoproxy records may fill a crucial gap in answering this question. In addition, modern instrumental data show that winter precipitation in the southwestern USA and Mexico are positively correlated with winter temperatures in Alaska and the Pacific Northwest (Mantua et al., 1997; Hare and Mantua, 2000). The signs of both sets of correlations are consistent with the positive relationships found between the PDO and tree-ring data from these areas (Biondi et al., 2001; D'Arrigo et al., 2001; MacDonald and Case, 2005). These linkages suggest that both centers of activity may require representation in paleoclimatic reconstructions of the PDO (Clement et al., 2009).

2.4 Conclusions

Our record demonstrates that over the last two millennia, there has been significant variability in the recurrence interval of the PDO, and strength in the PDO periodicities is intermittent over the past two millennia. The PDO appears to have been in positive phase during most of the Medieval Climate Anomaly (AD 800 to 1100), and negative phase during much of the Little Ice age, AD 1600-1900. Our data suggests that the greatest strength in PDO periodicities occurred from AD 1100 to 1350, 1500 to 1600, and 1800 to 1900. The persistence and recurrence of dominant climate periodicities remains a concern in predicting future variations across the Pacific Basin. Because the mode of variability of the PDO has apparently changed several times in the past two millennia, it may be expected to do so again in the future.

2.5 References

Barlow, M., Nigam, S., Berbery, E. H., 2001. ENSO, Pacific decadal variability, and US summertime precipitation, drought, and stream flow. Journal of Climate 14: 2105-2128.

Bennett, J., 1999. Paleoclimatic investigations from a closed-basin lake in southern interior British Columbia. MSc thesis, Queen's University, Ontario.

Benson, L., Linsley, B., Smoot, J., Mensing, S., Lund, S., Stine, S., Sarna-Wojcicki, A, 2003. Influence of the Pacific Decadal Oscillation on the climate of the Sierra Nevada, California and Nevada. Quaternary Research 59: 151-159.

Biondi, F., Gershunov, A., Cayan, D. R., 2001. North Pacific decadal climate variability since AD 1661. Journal of Climate 14: 5-10.

Chavez, F.P., Ryan, J., Lluch-Cota, S.E., Niquen, M., 2003. From anchovies to sardines and back: multidecadal change in the Pacific Ocean. Science 299: 217-221.

Clement, A.C., Burgman, R., Norris, J., 2009. Observational and model evidence for positive low-level cloud feedback. Science 325: 460-464.

D'Arrigo, R., Villalba, R., Wiles, G., 2001. Tree-ring estimates of Pacific decadal climate variability. Climate Dynamics 18: 219-224.

Finney, B.P., Gregory-Eaves, I., Douglas, M.S.V., Smol, J.P., 2002. Fisheries productivity in the northeastern Pacific Ocean over the past 2000 years. Nature 416: 729-733.

Francis, R.C., Hare, S.R., 1994. Decadal scale regime shifts in the large marine ecosystems of the North-east pacific: a case for historical science. Fisheries Oceanography 3: 279-291.

Gedalof, Z., Mantua, N. J., Peterson, D. L., 2002. A multi-century perspective of variability in the Pacific Decadal Oscillation: new insights from tree rings and coral. Geophysical Research Letters 29: 2204-2208.

Gedalof, Z., Peterson, D. L., Mantua, N. J., 2004. Columbia River flow and drought since 1750. Journal of the American Water Resources Association 40: 1579-1592.

Gedalof, Z., Smith, D. J., 2001. Interdecadal climate variability and regime-scale shifts in Pacific North America. Geophysical Research Letters 28: 1515-1518.

Gershunov, A., Barnett, T. P., 1998. Interdecadal modulation of ENSO teleconnections. Bulletin of the American Meteorological Society 79: 2715-2726.

Hare, S.R., Mantua, N.J., 2000. Empirical evidence for North Pacific regime shifts in 1977 and 1989. Progress in Oceanography 47: 103-145.

Howell, P., Pisias, N., Balance, J., Baughman, J., Ochs, L., 2006. ARAND time series analysis software. Brown University, Providence, RI.

Juillet-Leclerc, A., Schrader, H., 1987. Variations of upwelling intensity recorded in varved sediment from the Gulf of California during the past 3000 years. Nature 329: 146-148.

Kalnay, E., et al., 1996. The NCEP/NCAR 40-year reanalysis project. Bulletin of the American Meteorological Society 77: 437-472.

Kennett, J.P., Ingram, B. L., 1995. A 20,000-year record of ocean circulation and climate change from the Santa Barbara basin. Nature 277: 510-514.

Linsley, B. K., Wellington, G. M., Schrag, D. P., 2000. Decadal sea surface temperature variability in the subtropical south Pacific from 1726 to 1997 AD. Science 290: 1145-1148.

MacDonald, G.M., Case, R.A., 2005. Variations in the Pacific Decadal Oscillation over the past millennium. Geophysical Research Letters 32: L08703.

Mantua, N.J., Hare, S.R., Zhang, Y., Wallace, J.M., Francis, R.C., 1997. A pacific interdecadal climate oscillation with impacts on salmon production. Bulletin of the American Meteorological Society 78: 1069-1079.
McCrea, J.M., 1950. On the isotopic chemistry of carbonates and a paleotemperature scale. Journal of Chemical Physics 18: 849-857.
McKenzie, J.A., Hollander, D. J., 1993. Oxygen-isotope record in recent carbonate sediments from Lake Greifen, Switzerland (1750-1986). Geophysical Monograph 78: 101-111.
Minobe, S., 1997. A 50-70 year climatic oscillation over the North Pacific and North America. Geophysical Research Letters 24: 683-686.
Minobe, S., 1999. Resonance in bidecadal and pentadecadal climate oscillations over the North Pacific: role in climatic regime shifts. Geophysical Research Letters 26: 855-858.
Pienitz, R., Smol, J.P., Last, W.M., Leavitt, P.R., Cumming, B.F., 2000. Multiproxy Holocene paleoclimatic record from a saline lake in the Canadian Subarctic. The Holocene 10: 673-686.
Reimer, P.J., et al., 2009. Intcal09 and Marine09 radiocarbon age calibration curves, 0-50,000 years cal BP. Radiocarbon 51: 1111-1150.
Stuiver, M., 1970. Oxygen and carbon isotope ratios of freshwater carbonates as climatic indicators. Journal of Geophysical Research 75: 5247-5257.
Stuiver, M., Polach, H.A., 1977. Discussion: reporting of 14C data. Radiocarbon 19: 355-363.
Talbot, M.R., Kelts, K., 1990. Paleolimnological signatures from carbon and oxygen isotopic ratios in carbonates. American Association of Petroleum Geologists Memoir 50: 99-112.
Torrence, C., Compo, G.P., 1998. A practical guide to wavelet analysis. Bulletin of the American Meteorological Society 79: 61-78.
Vogel, J.S., Southon, J.R., Nelson, D.E., Brown, T.A., 1984. Performance of catalytically condensed carbon for use in accelerator mass spectrometry. Nuclear Instruments and Methods in Physics Research B5: 289-293.
Zhang, Y., Wallace, J. M., Battisti, D. S., 1997. ENSO-like interdecadal variability: 1900-93. Journal of Climate 10: 1004-1020.

CHAPTER 3

LINKING SOLAR ACTIVITY AND PACIFIC CLIMATE VARIABILITY

3.1 Background and Context

Solar variations on both decadal and centennial timescales have been associated with climate phenomena (van Loon et al., 2004; Hodell et al., 2001; White et al., 1997), but the mechanism remains controversial. The energy received by the Earth at the peak of the solar cycle increases by <0.1%, so the question has remained of how this could be amplified to produce an observable climate response. Recent modeling shows that the response of the Earth's climate system to the 11-year solar cycle may be amplified through stratosphere and ocean feedbacks and has the potential to impact climate variability on a number of timescales(Meehl et al., 2009). Here, we report a 1000-year record of changes in the stratigraphy and carbon isotope composition of varved lake sediment that shows variations in primary productivity on centennial timescales and suggests that solar activity may be an important component of Pacific climate variability.

Our sediment cores were taken from Isabela Crater Lake, (22°N, 106°W) in the subtropical northeast Pacific. We used an established productivity proxy (carbon isotope composition; $\delta^{13}C$) of the carbonate fine fraction (63-125 μm) of sediments to evaluate variability in primary productivity. Variations in the $\delta^{13}C$ of the CO_2 in the lake waters, which is recorded in the fine fraction of sediments, reflect the time-averaged primary production taking place in the euphotic zone (McKenzie, 1985). We also examined the stratigraphy of macroscopic carbonate layers for which a relation to increased primary productivity is inferred.

3.2 Results and Discussion

The carbonate stratigraphy and $\delta^{13}C$ values (Figure 3.1; Appendix A) show marked centennial oscillations. The $\delta^{13}C$ values oscillate around a mean value of -11‰, ranging from a high of -2‰ to a low of -16‰, indicating times of enhanced and reduced productivity, respectively. The most pronounced peaks in productivity occurred around AD 1750, 1575, 1350, 1175, and a cluster of peaks beginning at 1075.

The high productivity events in Isabela Crater Lake correspond to maxima in solar activity (Figure 3.1). Sensitivity experiments (Meehl et al., 2009) find that feedbacks between the stratosphere and ocean could produce a climate system response of the magnitude as seen in our observations. In their scenario, reduction in cloud cover by 2% during solar maxima acts to amplify the solar forcing, producing a slight (0.06°C) warming of ocean surface waters across the tropical Pacific, leading to enhanced evaporation and transport of water vapor by the trade winds to convergence zones. Increased precipitation in the convergence zones strengthens the Hadley and Walker circulations, with associated increases in trade winds and equatorial upwelling, leading to lower sea surface temperatures in the eastern equatorial Pacific (van Loon et al., 2004). Enhanced subsidence produces fewer clouds in the eastern equatorial Pacific and expands the subtropical regions, allowing even more solar radiation to reach the surface to produce a positive feedback (Pierrehumbert, 1995) that further magnifies the climate response (Meehl et al., 2009).

The proposed coupled response during solar maxima thus acts to keep the eastern equatorial Pacific cooler and drier than usual, producing conditions similar to a La Niña event. In the region around Isla Isabela, and similar to the relationships shown in Figure 3.1, peak solar

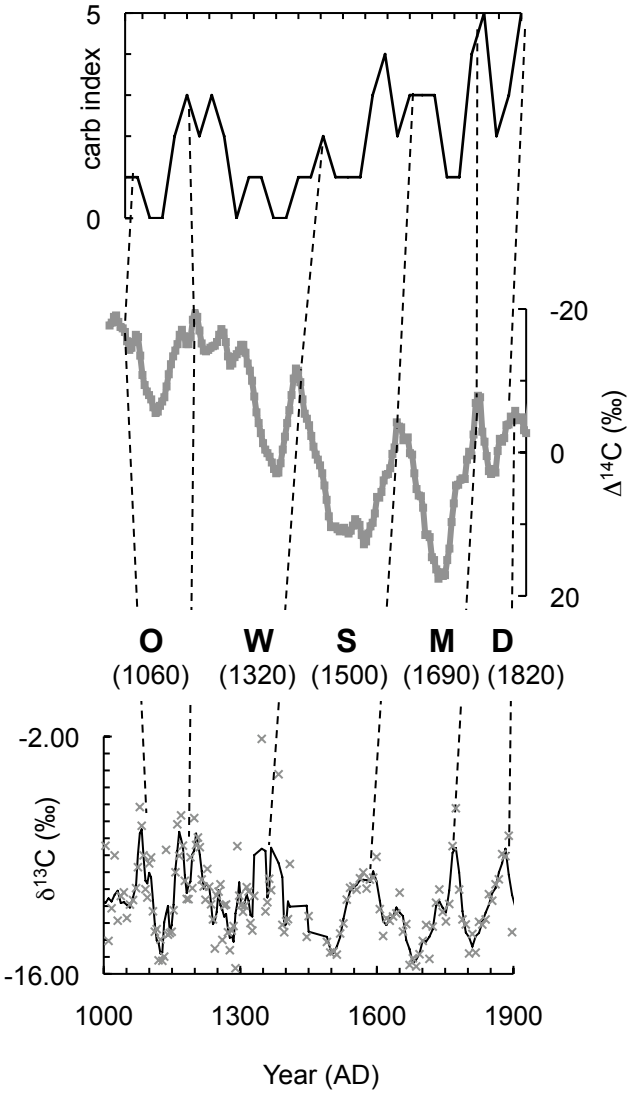


Figure 3.1. Productivity and solar records, top to bottom: coarse carbonate layers as a cluster index (number of layers per 10 cm); solar activity shown as $^{14}C/^{12}C$ ratios from the Intcal09 radiocarbon calibration curve (Reimer et al., 2009); individual measurements and three-point running mean of fine fraction sediment $\delta^{13}C$. Dashed lines show correlative depths and ages; chronology is based on eight AMS radiocarbon dates (Appendix B). The average interval between $\delta^{13}C$ samples is about 5 yr. Grand solar minima, centered on the years in parentheses (Bard et al., 1997) are labeled as follows: Oort (O); Wolf (W); Spörer (S); Maunder (M); Dalton (D). The 20th century is not shown due to the Seuss effect on atmospheric carbon.

years were characterized by decreased surface temperatures and suppressed precipitation (Meehl et al., 2009). This response has also been observed in adjacent areas during cold La Niña events (Gochis et al., 2007).

The correspondence between centennial climate variability and solar activity hint at a linkage between lake productivity and solar maxima. Downcore variations in sedimentological indices also indicate this possibility. This new subtropical Pacific record demonstrates that this ecosystem varied on centennial timescales over the past millennium, and these peaks in productivity correspond to decreased precipitation and maxima in solar activity. Although the role of solar activity in climate variations remains unclear, the convergence of model output and empirical evidence suggests the extent and amplitude of local hydrologic fluctuations may be more sensitive to solar forcing than was previously thought.

3.3 References

Bard, E., Raisbeck, G.M., Yiou, F., Jouzel, J., 1997. Solar modulation of cosmogenic nuclide production over the last millennium: comparison between 14C and 10Be records. Earth and Planetary Science Letters 150: 453-462.

Gochis, D.J., Brito-Castillo, L., Shuttleworth, W.J., 2007. Correlations between sea-surface temperatures and warm season streamflow in northwest Mexico. International Journal of Climatology 27: 883-901.

Hodell, D.A., Brenner, M., Curtis, J.H., Guilderson, T., 2001. Solar forcing of drought frequency in the Maya Lowlands. Science 292: 1367-1370.

McKenzie, J.A., 1985. Carbon isotopes and productivity in the lacustrine and marine environment. In Stumm, W. (ed.) Chemical Processes in Lakes: 99-118.

Meehl, G.A., Arblaster, J.M., Matthes, K., Sassi, F., van Loon, H., 2009. Amplifying the Pacific climate system response to a small 11-year solar cycle forcing. Science 325: 1114-1118.

Pierrehumbert, R.T., 1995. Thermostats, radiator fins, and the local runaway greenhouse. Journal of the Atmospheric Sciences 52(10): 1784-1806.

Reimer, P.J., et al., 2009. Intcal09 and Marine09 radiocarbon age calibration curves, 0-50,000 years cal BP. Radiocarbon 51: 1111-1150.

van Loon, H., Meehl, G.A., Arblaster, J.M., 2004. A decadal solar effect in the tropics in July-August. Journal of Atmospheric and Solar-Terrestrial Physics 66: 1767-1778.

White, W.B., Lean, J., Cayan, D.R., Dettinger, M.D., 1997. Response of global upper ocean temperature to changing solar irradiance. Journal of Geophysical Research 102(C2): 3255-3266.

CHAPTER 4

LATE HOLOCENE CLIMATE CHANGES ON ISLA ISABELA, GULF OF CALIFORNIA

Abstract

Sediments from Isabela crater lake, located on Isla Isabela in the southern Gulf of California, have been used to reconstruct changes in the precipitation and evaporation balance at the site over the past 6000 years. Using $\delta^{18}O$ as a proxy, the sediments record a number of pronounced dry periods at the site, indicated here as high $\delta^{18}O$ values, that coincide with cold SST in the eastern Pacific, and therefore an enhanced North Pacific High and generally dry conditions across western North America. Notable dry periods occur at approximately 5500, 4200, 3000, and 1200 cal BP, and may be tied to variations in the North Pacific Gyre system.

4.1 Introduction

Changing monsoon intensity is of broad regional importance because it is the primary source of water in a largely arid region of northwestern Mexico and the southwest US. In particular, the spatial heterogeneity that occurs from south to north as tropical signals propagate up the western Mexican coast into northern Mexico and the southwest US is of great concern for water resources for both nations. Changes in the strength and timing of the monsoon are frequently associated with floods and droughts, and at the most arid sites in this region, the interannual variability of summer climate can be larger than the mean summer rainfall itself (Higgins et al. 1998). Recent studies (e.g., Alcocer et al., 2000) have shown the groundwater supplies in parts of this region are dropping, resulting in increased reliance on annual precipitation and surface water supplies. Clearly, as reliance on this rainfall regime increases, so too does the importance of understanding the history and variations of the regional monsoon system.

Rainfall assumes critical importance for the Mexican economy. Both city reservoirs and much of Mexican agriculture depend on annual rains (Conde et al., 1997; Velasco, 1999; Englehart and Douglas, 2000). For example, severe drought conditions during the El Niño year of 1998 saw some seasonal precipitation totals less than 30% of normal. This created extreme hardships and environmental damage, including depleted reservoirs and extensive wildfires (Bell et al., 1999).

Recently, there was general agreement that the region of Mexico, Caribbean, and Central America showed significant drying in climate models estimating the effects of global warming on precipitation patterns (IPCC, 2007; Neelin et al., 2006). In many areas, water allocation policies and use are based on these types of models. Northwestern and central Mexico are predominantly agricultural, making them very socially and economically sensitive to changes in rainfall. Due to these immediate impacts, regional climate prediction has been widely identified as a key challenge in the next generation of climate models (IPCC, 2007). Adequate data are absolutely necessary to reach this goal, however, spatial and temporal coverage is poor across much of this region.

The North American Monsoon (NAM) is becoming an increasingly studied phenomenon (Douglas et al., 1993; Higgins et al., 1998; Leavitt et al., 2010), but the evolution of the NAM over long timescales is not well understood. Historical observations, similar to those conducted for the Indian Monsoon, have often been discontinuous, and near-instrumental records often are at too coarse resolution. Efforts are now underway to use tree ring reconstructions to understand past monsoon variability (e.g. Leavitt et al., 2010), but aside from tree ring records, resolution and chronological control remain a problem for many paleoclimate studies. In addition, records are far scarcer in the southeastern Gulf than other locations in the northern and western basins.

Lakes records often provide a means to understanding much longer (millennial) variability, and often at a resolution that is not possible in marine or terrestrial (middens, geomorphology etc.) records. The development of high resolution lake records on mainland Mexico has been accomplished in the Basin of Mexico and the Yucatan (Metcalfe et al., 2000; Hodell et al., 1995; 2001), but has been hindered in the core NAM region by dating problems, human disturbance, volcanic activity, and the limited number of varved lakes (Metcalfe, 1997; Metcalfe and Davies, 2007). Here we present a high-resolution, continuous record of $\delta^{18}O$ from lake sediments from Isla Isabela, a Pacific island off the coast of western Mexico. Lake records from central Mexico often reflect human disturbance over the past ~3500 years, as populations

migrated throughout the region and settled near water sources. The isolated location of Isla Isabela ensures human disturbance is minimal, and the continuous depositional record allows a reconstruction of changes in the NAM on decadal to millennial timescales.

4.2 Gulf Setting and North American Monsoon

The climate of the Gulf of California is monsoonal, with marked seasonal changes in wind direction and precipitation (Douglas et al., 1993; Adams and Comrie, 1997; Higgins et al., 1998). As a deep, narrow, northwest to southeast trending sea, the Gulf is bounded by the arid Baja California peninsula to the west and the Sonoran Desert to the east. The dry surroundings constrain its evaporative continental climate, in contrast with the more temperate marine climate commonly associated with the California Current.

The NAM is a pronounced increase in precipitation in boreal summer, as intense summer heating of the North American landmass results in a thermal low over the Mexican Plateau and southwestern US, resulting in a summer reversal of prevailing winds along the Gulf (Badan-Dangon et al., 1991) and transport of moist marine air on shore. Geographically, the NAM is centered over the Sierra Madre Occidental in northwestern Mexico, with summer rains extending into the southwestern United States. In these areas, monsoon rain accounts for a substantial portion of annual precipitation totals. Although the NAM is not as strong or persistent as its counterparts in Asia and Africa, the basic monsoon characteristics are shared, with essentially two modes, winter (cool and dry) and summer (wet and warm).

The winter (November to March) mode is dominated by strong northwesterly winds and lowered SSTs. The winds intensify in the fall as the North Pacific High (NPH) and the Intertropical Convergence Zone (ITCZ) retreat equatorward (Pares-Sierra et al., 2003; Bordoni et al., 2004), and the winds from the anticyclonic flow around the NPH are channeled down the axis of the Gulf by the high topography on both sides. The winter winds lower SST and generate upper ocean mixing and enhanced Ekman transport along the eastern margin of the Gulf (Alvarez-Borrego and Lara-Lara, 1991; Thunnell et al., 1996).

In contrast, the summer (April to October) mode introduces higher SST, higher humidity and rainfall. Northwesterly winds diminish as the NPH and ITCZ shift northward, and are replaced by irregular southerly winds (Bordoni et al., 2004). These southerly winds are modulated by "Gulf surges" that originate in cyclonic disturbances over the east Pacific warm pool off Central America and propagate northward into the subtropics. In the core of the summer monsoon (June to August), a combination of high elevation (mid-troposphere) winds, convective storms and Gulf surges transport moisture-laden tropical air into the Gulf and produce 60-80% of the annual rainfall (Bordoni and Stevens, 2005), with the majority of the rain concentrated along the western flank of the Sierra Madre Occidental and extending into the U.S. desert southwest (Douglas et al., 1993). The introduction of eastern tropical Pacific surface water by the Costa Rica Current, typically beginning in April-May (Castro et al., 2000) and the northward shift of the 28°C isotherm governs this northward propagation of convective storms and rainfall (Mitchell et al., 2002). By mid-summer, a layer of warm water (>28°C) up to 150 m thick covers the southern and central Gulf (Bray, 1988). During this time, wind-driven upwelling is weak and limited to the western side of the Gulf (Alvarez-Borrego and Lara-Lara, 1991; Bray and Robles, 1991).

Although the annual climate cycle of the region is generally a seesaw between the two monsoon modes, the duration and relative strength of each mode varies in response to insolation forcing on several timescales, from seasonal and interannual to centennial and millennial (e.g., Douglas et al., 2002, 2007; Barron et al., 2003, 2004; Herguera et al., 2003). Here, we explore how precipitation has varied over the past 6,000 years, and show that it has a wide range of natural variability, in addition to responding to forcing on multidecadal to millennial timescales.

4.3 Study Area

The sediment record presented here is from Lago Crater, on Isla Isabela (Figure 4.1). Isla Isabela is a small volcanic island (~200 ha) that formed during Pliocene rifting in the southern Gulf of California (Lyle and Ness, 1991). The crater lake is filled with a mix of fresh water from local precipitation and seawater percolating through the basalt. There are no other sources of water to the lake. Although weather data are not available for the island, Isla Isabela's present climate can be assumed to be similar to that of nearby San Blas, Nayarit, located approximately 60 km to the southeast (Figure 4.1). For the period 1971-2000, mean annual rainfall in San Blas was 1,400 mm, 95% of which fell from June to October (Figure 4.2). Mean monthly temperatures ranged from a low of 22ºC in January to a high of 29ºC August. Potential evaporation was highest in the late spring and dropped slightly during the summer; for the year as a whole, average evaporation exceeded precipitation by 600 mm (Figure 4.2; Mexico Comisión Nacional del Agua, http://smn.cna.gob.mx). Sea surface temperatures (SST) in this section of the Gulf range from 23ºC in late winter to 28ºC in late summer (Reynolds and Smith, 1994).

Lago Crater has a surface area of 6 ha and a maximum depth of 24 m in the depocenter (Kienel et al., 2010; Alcocer et al., 1998). The limnological surveys of Kienel et al. (2010) and Alcocer et al. (1998) have demonstrated that Lago Crater is meromictic, with increasing salinity at depth (~60-70‰). In addition, waters are slightly alkaline throughout (pH = 7.5) and anoxic below ~5 m (Kienel et al., 2010; Alcocer et al., 1998).

Lake sediments consist of alternating light and dark laminations (Figure 4.3). The light laminations are composed of carbonates, organic material from algae and bacteria, ostracod shells and varying amounts of clastic material. The dark laminations are composed of organic material, principally from algae and bacteria. Episodic coarse layers of carbonate also occur.

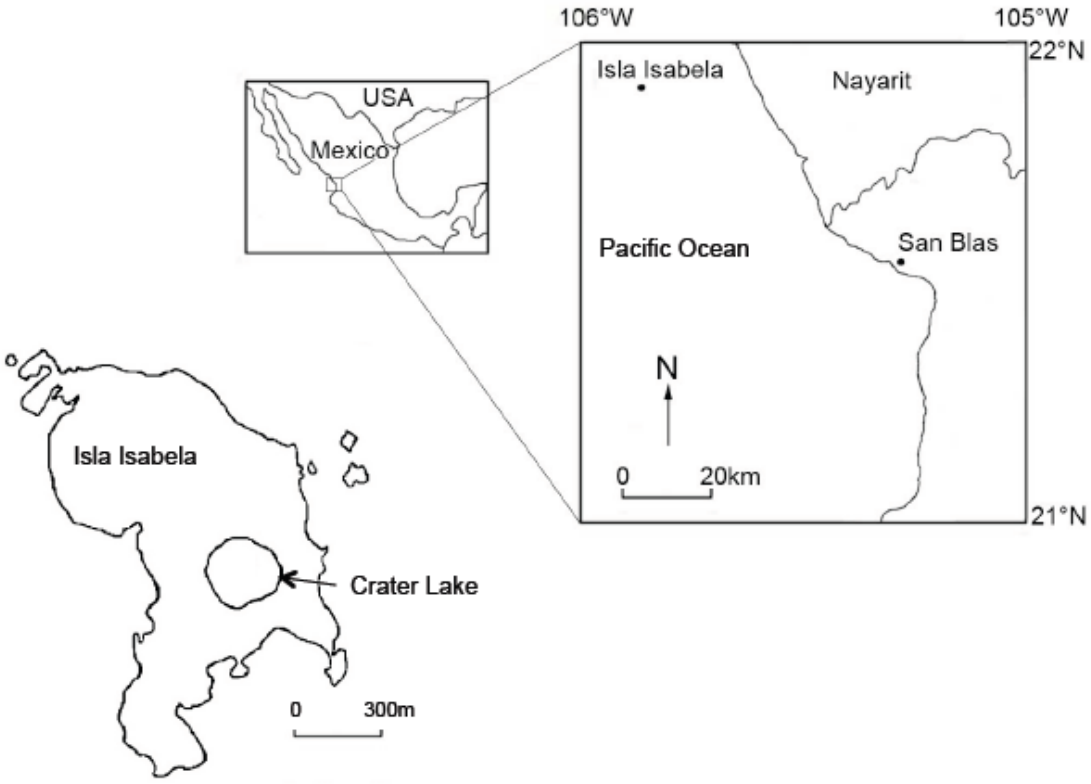


Figure 4.1. Isla Isbela (22°N, 106°W) is located off the coast of Nayarit, Mexico.

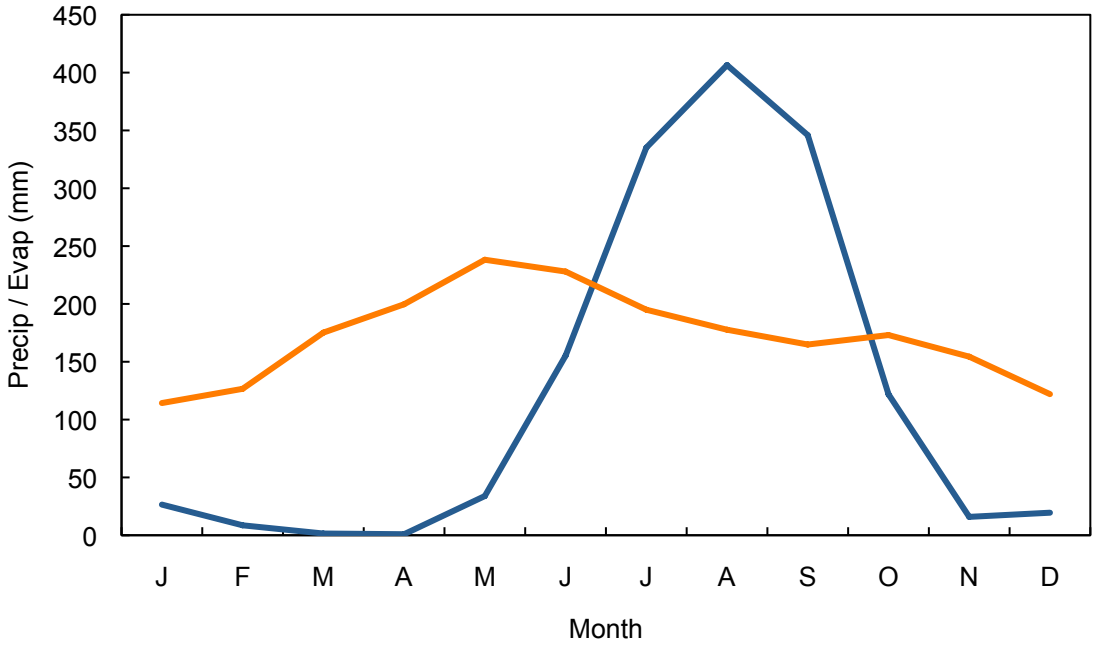


Figure 4.2. Monthly average precipitation (blue) and evaporation (orange) totals at San Blas, Nayarit for the period 1971-2000 (Mexico Comisión Nacional del Agua, http://smn.cna.gob.mx). There is a strong seasonality in precipitation in this region, with maximum precipitation from July to September, and a pronounced minimum from December to April.



Figure 4.3. Isabela core top, showing mm-scale varves. Section is approximately 65 cm long.

4.4 Methods

Overlapping cores were recovered from Lago Crater in 2004 and 2006, and all cores were split, imaged, and sampled at the German Research Centre for Geosciences (GFZ), in Potsdam, Germany. Cores were sampled at 1-3 cm intervals over the entire core length, and mm-scale lamina couplets were sampled through the top 12 cm. In addition, surface water samples were collected from the crater lake in November 2006.

Surface waters were analyzed for oxygen, deuterium, and strontium isotopic compositions. For oxygen and deuterium analyses, a 200 mL sample was introduced using an AquaPrep automated device attached to a GV IsoPrime isotope ratio mass spectrometer. Oxygen and deuterium isotopic data are reported in the d notation relative to Standard Mean Ocean Water (SMOW). The precision for each analysis is ±0.05‰ for oxygen and ±1.00‰ for deuterium.

Strontium isotopic measurements were obtained using a VG Sector 54 solid source mass spectrometer equipped with 8 faraday cups located at the Center for Isotope Geochemistry at University of California, Berkeley. Isotopic ratios were collected using a multi-dynamic measurement routine and were corrected for mass fractionation using an exponential correction and the accepted $^{86}Sr/^{88}Sr = 0.1194$. The long-term mean $^{87}Sr/^{86}Sr$ for NBS 987 is 0.71029 +/- 0.00001.

Strontium concentrations were determined by standard isotope dilution techniques using an enriched ^{84}Sr isotopic spike from Oak Ridge National Laboratory. Uncertainty of isotope dilution measurements is estimated at 1% based on spike calibrations with well-characterized natural rock standards.

Sediment samples were wet sieved and the 63-125 mm fraction was dried at 40°C overnight prior to stable isotope analysis of the bulk inorganic carbonate. Samples were analyzed for $\delta^{18}O$ on a GV Instruments JB Series Isoprime mass spectrometer with a dual inlet multiprep system optimized for analysis of small carbonate samples. For isotope analysis, 0.1-0.5 mg carbonate was reacted with phosphoric acid to produce CO_2 following the method of McCrea (1950). Oxygen isotope data are reported in the d notation relative to the Pee Dee Belemnite (PDB) standard. The internal precision of the $\delta^{18}O$ measurements is ±0.05‰, and repeated measurements had a standard deviation of 0.5‰.

An AMS radiocarbon chronology was established using ~1 mg samples of bulk acid insoluble organic matter. Sediment samples were acidified at 90°C using 1N HCl, rinsed with distilled water to neutral pH, and dried overnight. Following combustion to CO_2, samples were reduced to graphite using iron as a catalyst, after Vogel et al. (1984). A standard coal blank was treated simultaneously with the samples and used for background subtraction. Radiocarbon content was measured at the Center for Accelerator Mass Spectrometry (CAMS), at Lawrence Livermore National Laboratory. Radiocarbon content is reported following standard conventions (Stuiver and Polach, 1977; Reimer et al., 2009), and includes a $\delta^{13}C$ correction of -23‰.

4.5 Results

4.5.1 Water Isotopic Composition

Oxygen, deuterium, and strontium contents of surface water and rain are shown in Table 4.1. In addition, $\delta^{13}C$ of Lago Crater surface water has been reported as -15‰ VPDB (Kienel et al., 2010). The composition of Lago Crater surface water does not appear to vary spatially. Mean $\delta^{18}O$ was 2.47 ± 0.03‰, while mean δD was 0.06 ± 0.4‰. This is in contrast with the weighted annual precipitation, reported as -8‰ $\delta^{18}O$ and -54‰ δD (IAEA, 2001). The strontium isotopic ratio of surface water averaged 0.70908 ± 2E-5, and the mean strontium concentration was 11.0 ± 1.5 ppm.

Table 4.1. Composition of surface water and rain collected during November 2006 on Isla Isabela. Surface water samples were collected from five different locations in Lago Crater. Oxygen and deuterium isotopic ratios are reported as per mil VSMOW; strontium isotopic ratios are reported with 2σ error; strontium concentrations are reported in parts per million.

Sample	$\delta^{18}O$ (‰ VSMOW)	δD (‰ VSMOW)	$^{87}Sr/^{86}Sr$	2σ	[Sr] (ppm)	± (ppm)
MXIS 1	2.49	-0.43	0.7090900	1.00E-05	9.0	0.1
MXIS 2	2.45	-0.05	0.7091100	1.00E-05	13.1	0.13
MXIS 3	2.49	0.56	0.7090450	2.00E-05	10.9	0.1
MXIS 4	2.45	0.07	0.7090710	3.00E-05	10.4	0.1
MXIS 5	2.49	0.15	0.7090725	4.70E-05	11.4	0.1
MXIS Rain	-0.24	4.28	*	*	*	*

*Not analyzed for Sr content

4.5.2 Chronology

We used 14 AMS radiocarbon dates to establish a sediment chronology for the last 6000 years. Radiocarbon ages together with their converted calendar year ages are shown in Table 4.2. A tephra layer located at 1.6 cm sediment depth corresponds to the 1998-1999 eruption of the Colima volcano, confirming that the top core sections accurately captured the sediment-water interface. The radiocarbon ages indicate near-linear sedimentation rates during the last 6000 y, with an average rate of 2.6 mm/y. However, an age of 360±35 ^{14}C yr BP was obtained from surface sediments, indicating that there is a source of pre-aged carbon in the lake or catchment. This age represents a weighted average of organic matter inputs to the lake, and reflects both the regional marine carbon reservoir effect (from seabird guano input to the lake; 910±60 ^{14}C yr BP, Ingram and Southon, 1996), primary productivity and recycling of organic matter within the water column, and terrestrial inputs from the catchment. The ΔR of 360 ^{14}C yr BP was assumed to be constant over this core section, and calibrated ages were determined using CALIB 6.0 (Reimer et al., 2009). The ARAND software program was used to interpolate between calibrated radiocarbon ages (Howell, et al., 2006).

Table 4.2. Raw radiocarbon and calibrated ages of the acid insoluble fraction of bulk sediments.

CAMS #	Depth (cm)	^{14}C age (^{14}C yr BP)	±	1σ cal age range (cal BP)	2σ cal age range (cal BP)	Median probability age (cal BP)
136255	12	360	35	-	-	-
140535	78	580	35	149-186	138-223	182
140536	178	1105	35	661-693	652-730	680
140537	278	1445	35	934-987	930-1018	982
140538	280	1450	35	953-1000	932-1056	988
140539	380	2105	35	1605-1700	1549-1718	1645
140540	481	2445	35	1995-2066	1949-2135	2045
140541	580	2675	35	2311-2352	2300-2359	2330
140542	680	3010	35	2743-2774	2721-2798	2760
140543	780	3500	35	3332-3392	3316-3412	3359
140545	882	3925	35	3826-3900	3808-3928	3850
140546	1080	4515	35	4611-4711	4569-4826	4688
140547	1180	5095	35	5330-5578	5325-5583	5468
131375	1271	5490	40	5761-5809	5749-5830	5834

4.5.3 Sediment $\delta^{18}O$

Individual varves were sampled over the core top (0-12 cm), and the stable oxygen isotopes of authigenic carbonate in the fine fraction were analyzed (Figure 4.4). Over the 30 years represented by the core section, $\delta^{18}O$ values ranged from a low of approximately -2‰, to a high of approximately 2‰, with a mean of about 0‰. Annual precipitation totals over this time period ranged from 800 mm in 1994 to 2200 mm in 1998. Over the entire composite core, $\delta^{18}O$ ranged from a minimum of -6‰ to a maximum of 5‰ (Figure 4.5; Appendix A). A long-term trend of approximately 2‰ occurs, and the highest values occur in the older portion of the record, while the lowest values occur in the youngest sediments.

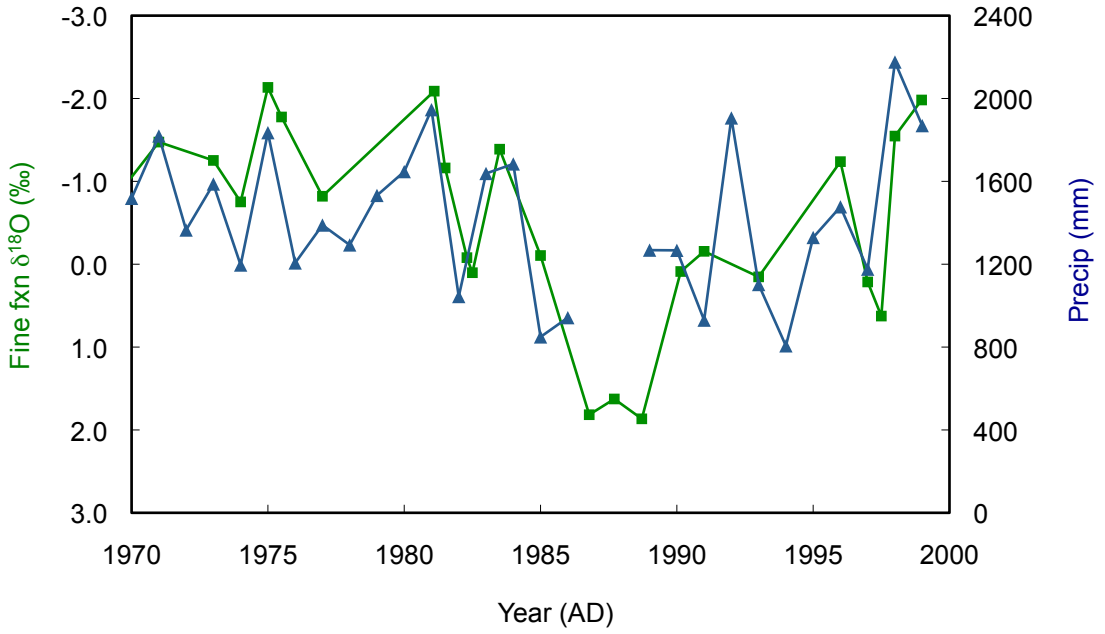


Figure 4.4. $\delta^{18}O$ (green) of individual varves in the core top correspond to the annual precipitation totals (blue) for San Blas, with generally lower $\delta^{18}O$ values during years with higher precipitation and vice versa. Precipitation data were provided by the Mexico Comisión Nacional del Agua (CONAGUA; http://smn.cna.gob.mx).

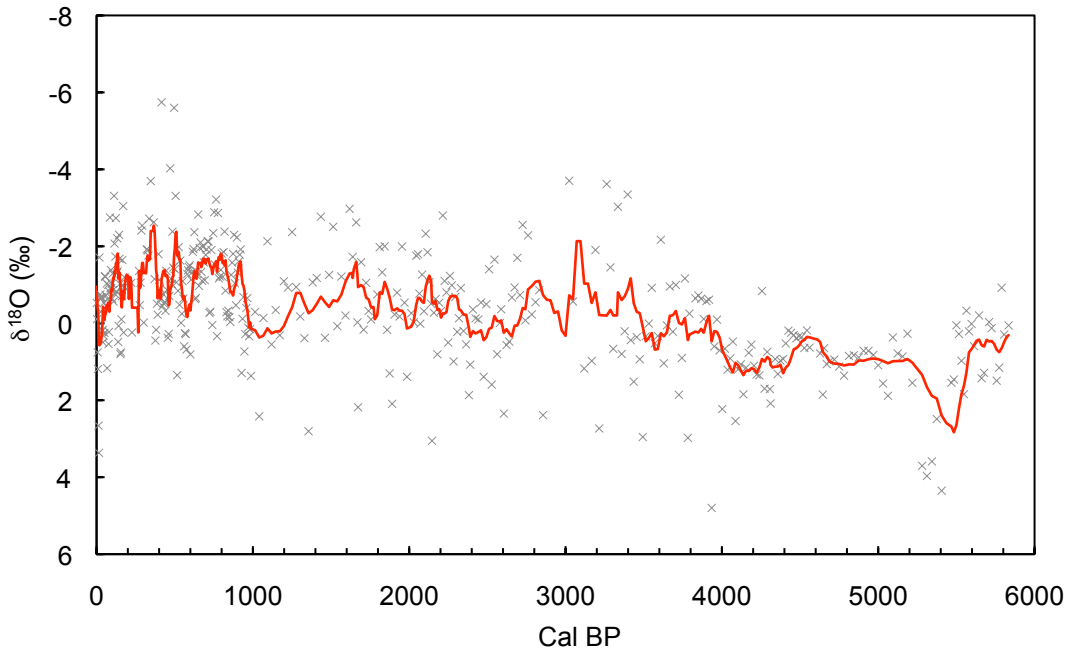


Figure 4.5. Individual $\delta^{18}O$ measurements (crosses) and 9-point running mean (red line) of sediments from Isabela crater lake.

4.6 Discussion

The highly stratified lake on Isla Isabela exhibits permanent anoxia in the subsurface water and confines phytoplankton, dominated by dinoflagellates and diatoms, to the oxygenated surface water. Although the island is volcanic, the strontium composition of Lago Crater surface water (0.70908) shows that the water is primarily marine in origin when compared to the average seawater strontium isotope ratio of 0.709189 (DePaolo and Ingram, 1985). Although the lake water is currently a mix of infiltrating ocean water and freshwater precipitation, infiltration is relatively slow and the lake is strongly affected by evaporation, as evidenced by the elevated strontium concentration of Lago Crater (11.0 ppm) relative to average seawater (8 ppm).

The pattern of precipitation over the year in San Blas reflects the North American Monsoon (Figure 4.2). There is a strong seasonality in precipitation in this region, with a pronounced maximum in precipitation July to September, and a minimum from December to April. Lake carbonates were presumed to precipitate in the euphotic zone during the summer (Kienel et al., 2010), and measurements of $\delta^{18}O$ in individual varves in the core top correspond to annual precipitation totals for San Blas (Figure 4.4). There are missing data in the San Blas precipitation record for 1987 and 1988, however lower $\delta^{18}O$ values generally occur during years with higher precipitation and higher $\delta^{18}O$ values occur during years with lower precipitation. There are not observable differences in either the monthly distribution of precipitation or monthly temperatures that would indicate that $\delta^{18}O$ is responding to regional source or temperature effects (CONAGUA, data not shown). Given these constraints on the $\delta^{18}O$, and the fact that there are no surface inputs to or outputs from the lake, we conclude that the $\delta^{18}O$ primarily reflects the balance between precipitation from the NAM and evaporation.

Over the past 6000 years, the $\delta^{18}O$ shows a range of approximately 11‰, but the range of values changes through time, with some periods showing a wider spread between minimum and maximum, while other periods are quieter, with a smaller range. For example, the period from 3000 to 1000 cal BP appears to have greater scatter and higher frequency variability than the period after 1000 cal BP. This is characteristic of sediment oxygen isotope records in closed basin lakes (e.g., Kirby et al., 2004), and reflects changes in the basin hydrology through time.

One of the most pronounced features of the record is the prolonged maximum in $\delta^{18}O$ at approximately 5500 cal BP, suggesting prolonged dry conditions lasting about 200 years. Many records have shown that there was a sudden and widespread shift in precipitation 5500 to 5300 cal BP. Changes in insolation have been tied to the mid-Holocene drying of Saharan Africa (deMenocal et al., 2000), with decreasing insolation resulting in reduced monsoon rainfall, leading eventually to the decline of vegetation and transition to desert conditions (Hoelzmann et al., 1998). Reconstructions for the tropical Pacific during the mid-Holocene suggest that tropical Pacific SST were generally colder in the eastern part of the basin, consistent with the occurrence of weaker and less frequent El Nino events (Koutavas et al., 2006; Barron and Anderson, 2010; Marchitto et al., 2010).

Another prolonged dry period occurs in the Isabela record, beginning around 4200 cal BP. There is evidence for arid and cold conditions around 4200 cal BP at several sites across the North Atlantic, northern Africa and southern Asia (e.g., Bond et al., 1997; Bianchi and McCave, 1999; deMenocal et al., 2000; Cullen et al., 2000). This period coincides with the collapse of a number of major urban civilizations across northern Africa and central Asia (Cullen et al., 2000; deMenocal, 2001). Cullen et al. (2000) show that at about 4025 yr BP and for the subsequent

300 years there was a significant increase in the amount of dust reaching the Gulf of Oman, suggesting a period of extreme drought across Mesopotamia and the Tigris and Euphrates flood plains. Cooler SST are found during this time period in the eastern equatorial Pacific (Koutavas et al., 2006) as well as the Soledad Basin, off of Baja California Sur (Marchitto et al., 2010).

The period from 3000 to 2700 cal BP also appears to have been drier than today, and is followed by a period of relatively variable conditions over the next millennium. This ends with a pronounced dry period during the Medieval Climate Anomaly (MCA), 1200 to 1000 cal BP. The MCA and Little Ice Age (LIA) are generally regarded as the largest broad-scale deviations of climate change in the last several thousand years. Although the MCA was anomalously warm in the North Atlantic and Europe, there is evidence for a cool eastern Pacific and dry conditions over western North America (Mann and Jones, 2003; Graham et al., 2007). Cook et al. (2004) documented widespread dry conditions that extended throughout much of the west between 1100 and 700 yr BP, and compilations by MacDonald and Case (2005) and Graham et al. (2007) support La Nina-like winter Northern Hemisphere circulation patterns during the MCA. On Isabela, the MCA was generally dry, and ended with an abrupt step to wetter conditions at 950 cal BP. Although there appears to be a general drying trend over much of the past millenium, no clear signature is observed at Isabela during the period assigned to the LIA (~650 to 100 yr BP).

The relationships between western drought and La Nina-like conditions largely stem from the association of anomalously low SST with anomalously high pressure throughout the eastern Pacific, extending from the tropical Pacific to the Gulf of Alaska (Herweijer et al., 2006). In contrast, El Nino events and positive PDO phases are associated with an enhanced Aleutian low and strengthened cyclonic circulation in the North Pacific that result in greater poleward transport, and higher SST throughout the eastern Pacific. Modeling results also point to the cool SST-drought relationship: Herweijer et al. (2006) applied an atmospheric GCM to the tree-ring database and tropical Pacific coral SST record of Cobb et al. (2003) to argue that severe Western droughts of the latter half of the 19th century were linked with anomalously cool tropical Pacific SSTs. Conditions during the LIA further support this relationship: warmer SST in the eastern Pacific during the LIA has been linked with increased precipitation in much of western North American (Barron and Anderson, 2010; Graham et al., 2007).

A 1500-year variation during the Holocene was first recognized in North Atlantic cores that showed variations in ice-rafted debris (Bond et al. 1997). But few climate records have shown a clear 1500-year period in the Holocene. Recently, SST minima from a core in the midlatitude North Pacific have revealed a correspondence with the Bond events (Isono et al., 2009). Further, Barron et al. (2003) observed changes in SST along the California margin at ODP Site 1019, that had a periodicity of 1470-1820 years. Isono and coauthors (2009) suggested that changes in the North Pacific gyre system were responsible for the dominant periodicities they observed, leading to high coherence between the Japan and California margins. This would also impact Isabela, which is influenced by the latitudinal extent of the California Current. During times when the current is further south, drier conditions prevail at Isabela, and vice versa.

4.7 Conclusions

This $\delta^{18}O$ record from Isabela crater lake reflects changes in precipitation at the site over the past 6000 years. There have been a number of pronounced dry periods at the site, indicated here as high $\delta^{18}O$ values, that coincide with cold SST in the eastern Pacific, and therefore an

enhanced North Pacific High and generally dry conditions across western North America. Notable dry periods occur at approximately 5500, 4200, 3000, and 1200 cal BP, and may be tied to variations in the North Pacific Gyre system.

4.8 References

Adams, D.K., Comrie, A.C. 1997. The North American monsoon. Bulletin of the American Meteorological Society 78(10): 2197-2213.

Alcocer, J., Escobar, E., Lugo, A. 2000. Water use (and abuse) and its effects on the crater-lakes of Valle de Santiago, Mexico. Lakes & Reservoirs: Research and Management 5: 145-149.

Alcocer, J., Lugo, A., Rosario Sanchez, M., Escobar, E. 1998. Isabela crater-lake: a Mexican insular saline lake. Hydrobiologia 381: 1-7.

Alvarez-Borrego, S., Lara-Lara, J.R. 1991. The physical environment and primary productivity of the Gulf of California. In Dauphin, J.P., Simoneit, B.R.T. (eds.) The Gulf and Peninsular Provinces of the Californias. AAPG Memoir 47: 555-568.

Badan-Dangon, A., Dorman, C.E., Merrifield, M.A., Winant, C.D. 1991. The lower atmosphere over the Gulf of California. Journal of Geophysical Research 96(C9): 16,877–16,896.

Barron, J.A., Anderson, L., 2010. Enhanced late Holocene ENSO/PDO expression along the margins of the eastern North Pacific. Quaternary International (in press).

Barron, J.A., Bukrya, D., Bischoff, J.L. 2004. High resolution paleoceanography of the Guaymas Basin, Gulf of California, during the past 15 000 years. Marine Micropaleontology 50(3-4): 185-207.

Barron, J.A., Bukry, D., Bischoff, J.L. 2003. A 2000-yr-long record of climate from the Gulf of California. In West, G.J. and Blomquist, N.L. (eds.) Proceedings of the Nineteenth Pacific Climate Workshop, Asilomar, Pacific Grove, CA, March 3-6, 2002.

Bell, G. D., Halpert, M. S., Ropelewski, C. F., Kousky, V. E., Douglas, A. V., Schnell, R. C., Gelman, M. E. 1999. Climate assessment for 1998. Bulletin of the American Meteorological Society 80: S1–S48.

Bianchi, G.G., McCave, I.N. 1999. Holocene periodicity in North Atlantic climate and deep-ocean flow south of Iceland. Nature 397: 515-517.

Bond, G., Showers, W., Cheseby, M., Lotti, R., Almasi, P., deMenocal, P., Priore, P., Cullen, H., Hajdas, I., Bonani, G., 1997. A pervasive millennial-scale cycle in North Atlantic Holocene and glacial climates. Science 278: 1257-1266.

Bordoni, S., Ciesielski, P.E., Johnson, R.H., McNoldy, B.D., Stevens, B. 2004. The low-level circulation of the North American Monsoon as revealed by QuikSCAT. Geophysical Research Letters 31: L10109.

Bordoni, S., Stevens, B. 2005. Principal component analysis of the summertime winds over the Gulf of California: a gulf surge index. Monthly Weather Review 134: 3395-3414.

Bray, N.A. 1988. Thermohaline circulation in the Gulf of California. Journal of Geophysical Research 93(C5): 4993–5020.

Bray, N.A., Robles, J.M. 1991. Physical oceanography of the Gulf of California. In Dauphin, J.P., Simoneit, B.R.T. (eds.) The Gulf and Peninsular Provinces of the Californias. AAPG Memoir 47: 511-554.

Castro, C.L., McKee, T.B., Pielke, R.A. 2000. The relationship of the North American Monsoon to tropical and north Pacific sea surface temperatures as revealed by observational analyses. Journal of Climate 14: 4449-4473.

Cobb, K.M., Charles, C.D., Cheng, H., Edwards, R.L., 2003. El Nino/Southern Oscillation and tropical Pacific climate during the last millennium. Nature 424: 271-276.

Cook, E.R., Woodhouse, C.A., Eakin, C.M., Meko, D.M., Stahle, D.W., 2004. Long-term aridity changes in the western United States. Science 306: 1015-1018.

Conde, C., Liverman, D., Flores, M., Ferrer, R., Araújo, R., Betancourt, E., Villareal, G., Gay, C. 1997. Vulnerability of rainfed maize crops in Mexico to climate change. Climate Research 9: 17–23.

Cullen, H.M., deMenocal, P.B., Hemming, S., Hemming, G., Brown, F.H., Guilderson., T., Sirocko, F., 2000. Climate change and the collapse of the Akkadian empire: Evidence from the deep sea. Geology 28(4): 379-382.

deMenocal, P., Ortiz, J., Guilderson, T., Sarnthein, M., 2000. Coherent high- and low-latitude climate variability during the Holocene warm period. Science 288: 2198-2202.

deMenocal, P.B., 2001. Cultural responses to climate change during the late Holocene. Science 292: 667-672.

DePaolo, D.J., Ingram, B.L., 1985. High-resolution stratigraphy with strontium isotopes. Science 227: 938-941.

Douglas, M.W., Maddox, R.A., Howard, K. 1993. The Mexican Monsoon. Journal of Climate 6: 1665-1677.

Douglas, R.G., Gorsline, D., Grippo, A., Granados, I., Gonzalez-Yajimovich, O. 2002. Holocene ocean-climate variation in Alfonso Basin, Gulf of California, Mexico. In West, G.J., Buffaloe, L.D. (eds.) Proceedings of the Eighteenth PACLIM Workshop. Asilomar, Pacific Grove, CA, pp. 7-20.

Douglas, R., Gonzalez-Yajimovich, O., Ledesma-Vazquez, J., Staines-Urias, F. 2007. Climate forcing, primary production and the distribution of Holocene biogenic sediments in the Gulf of California. Quaternary Science Reviews 26: 115-129.

Englehart, P. J. and Douglas, A. V. 2000. Dissecting the macro-scale variations in Mexican maize yields (1961–1997). Geographical and Environmental Modelling 4: 65–81.

Graham, N.E., et al., 2007. Tropical Pacific-mid-latitude teleconnections in medieval times. Climatic Change 83: 241-285.

Herguera, J.C., Franco, G.B., Molina-Cruz, A. 2003. Decadal surface ocean variability in the lower Gulf of California: records for the past 300 years. Geofisica Internacional 42(3): 397-406.

Herweijer, C., Seager, R., Cook, E.R., 2006. North American droughts of the mid to late nineteenth century: a history, simulation and implication for Mediaeval drought. The Holocene 16(2): 159-171.

Higgins, R.W., Mo, K.C., Yao, Y. 1998. Interannual variability of the U.S. summer precipitation regime with emphasis on the southwestern monsoon. Journal of Climate 11: 2582-2606.

Hodell, D.A., Curtis, J.H., Brenner, M., 1995. Possible role of climate in the collapse of Classic Maya civilization. Nature 375: 391-394.

Hodell, D.A., Brenner, M., Curtis, J.H., Guilderson, T., 2001. Solar forcing of drought frequency in the Maya Lowlands. Science 292: 1367-1370.

Hoelzmann, P., Jolly, D., Harrison, S.P., Laarif, F., Bonnefille, R., Pachur, H.J., 1998. Mid-Holocene land surface conditions in northern Africa and Arabian Peninsula. Global Biogeochemical Cycles 12(1): 35-51.

Howell, P., Pisias, N., Balance, J., Baughman, J., Ochs, L., 2006. ARAND time series analysis software. Brown University, Providence, RI.

IAEA. 2001. GNIP Maps and Animations. International Atomic Energy Agency, Vienna. Accessible at http://isohis.iaea.org

Ingram, B.L., Southon, J.R. 1996. Reservoir ages in eastern Pacific coastal and estuarine waters. Radiocarbon 38(3): 573-582.

IPCC, 2007, Climate change 2007: the physical science basis. Contribution of Working Group 1 to the Fourth Assessment Report of the Intergovernmental Panel on Climate Change. Solomon, S., Qin, E., Manning, M., Chen, A., Marquis, M., Averty K.B., Tignor, M., Miller, H.L., (eds.). Cambridge Univ. Press, Cambridge, UK.

Isono, D., Yamamoto, M., Irino, T., Oba, T., Murayama, M., Nakamura, T., Kawahata, H., 2009. The 1500-year climate oscillation in the midlatitude North Pacific during the Holocene. Geology 37: 591-594.

Kirby, M.E., Poulsen, C.J., Lund, S.P., Patterson, W.P., Reidy, L., Hammond, D.E., 2004. Late Holocene lake level dynamics inferred from magnetic susceptibility and stable oxygen isotope data: Lake Elsinore, souther California (USA). Journal of Paleolimnology 31: 275-293.

Kienel, U., Plessen, B., Schettler, G., Weise, S., Pinkerneil, S., Böhnel, H., Englebrecht, A., Byrne, R., Haug, G., 2010. Sensitivity of the saline crater lake on Isla Isabel (Nayarít, México) to seasonal precipitation / evaporation contrast and seabird activity. (submitted)

Koutavas, A., deMenocal, P.B., Olive, G.C., Lynch-Stieglitz, J., 2006. Mid-Holocene El Nino-Southern Oscillation (ENSO) attenuation revealed by individual foraminifera in eastern tropical Pacific sediments. Geology 34: 993-996.

Leavitt, S.W., Woodhouse, C.A., Castro, C.L., Wright, W.E., Meko, D.M., Touchan, R., Griffin, D., Ciancarelli, B., 2010. The North American Monsoon in the U.S. Southwest: potential for investigation with tree-ring carbon isotopes. Quaternary International (in press).

Lyle, M., Ness, G.E., 1991. The opening of the southern Gulf of California. In Dauphin, J.P., Simoneit, B.R.T. (eds.) The Gulf and Peninsular Province of the Californias. AAPG Memoir 47: 403-423.

MacDonald, G.M., Case, R.A., 2005. Variations in the Pacific Decadal Oscillation over the past millennium. Geophysical Research Letters 32, L08703.

Mann, M.E., Jones, P.D., 2003. Global surface temperatures over the past two millennia. Geophysical Research Letters 30: 1820-1823.

Marchitto, T.M., Muscheler, R., Ortiz, J.D., Carriquiry, J.D., van Geen, A., 2010. Dynamical response of the tropical Pacific Ocean to solar forcing during the early Holocene. Science 330: 1378-1381.

McCrea, J.M., 1950. On the isotopic chemistry of carbonates and a paleotemperature scale. Journal of Chemical Physics 18, 849-857.

Metcalfe, S.E., Bimpson, A., Courtice, A.J., O'Hara, S.L., Taylor, D.M., 1997. Climate change at the monsoon/Westerly boundary in Northern Mexico. Journal of Paleolimnology 17: 155-171.

Metcalfe, S., Davies, S., 2007. Deciphering recent climate change in central Mexican lake records. Climatic Change 83: 169-186.

Metcalfe, S.E., O'Hara, S.L., Caballero, M., Davies, S.J., 2000. Records of Late Pleistocene-Holocene climatic change in Mexico- a review. Quaternary Science Reviews 19: 699-721.

Mitchell, D.L., Ivanova, D., Rabin, R., Brown, T.J., Redmond, K. 2002. Gulf of California sea surface temperatures and the North American monsoon: mechanistic implications from observations. Journal of Climate 15: 2261-2281.

Neelin, J.D., Munnich, M., Su, H., Meyerson, J.E., Holloway, C. 2006. Tropical drying trends in global warming models and observations. Proceedings of the National Academy of Sciences 103(16): 6110-6115.

Pares-Sierra, A., Mascarenhas, A., Marinone, S.G., Castro, R. 2003. Temporal and spatial variation of the surface winds in the Gulf of California. Geophysical Research Letters 30(6): 1312-1315.

Reimer, P.J., et al., 2009. Intcal09 and Marine09 radiocarbon age calibration curves, 0-50,000 years cal BP. Radiocarbon 51, 1111-1150.

Reynolds, R.W., Smith, T.M., 1994. Improved global sea surface temperature analyses using optimum interpolation. Journal of Climate 7: 929-948.

Stuiver, M., Polach, H.A., 1977. Discussion: reporting of 14C data. Radiocarbon 19, 355-363.

Thunell, R., Pride, C., Tappan, E., Muller-Karger, F.E. 1996. Plankton response to physical forcing in the Gulf of California. Journal of Plankton Research 18: 2017-2026.

Velasco, I. 1999. Severe droughts becoming recurrent, more persistent in Mexico. Drought Network News 11(1): 3–6.

Vogel, J.S., Southon, J.R., Nelson, D.E., Brown, T.A., 1984. Performance of catalytically condensed carbon for use in accelerator mass spectrometry. Nuclear Instruments and Methods in Physics Research B5, 289-293.

CHAPTER 5

CONCLUSIONS

5.1 Conclusions

Many paleo proxy studies have been employed in both the marine and terrestrial settings in and around the Gulf of California. However, the record from Isla Isabela is unique in its high resolution, temporal continuity, and lack of human impact over the late Holocene. The studies comprising this thesis have illustrated that the climate of this region has varied on several timescales. In Chapter 2, the oxygen isotope record showed variability in the Pacific Decadal Oscillation over the last two millennia. This apparent waxing and waning in the strength of the PDO has not been recognized previously, and suggests that this mode of variability may be nonstationary in time. This represents an important consideration when comparing proxy records to model output for future projections. In Chapter 3, changes in productivity in the lake showed a correspondence with solar activity that hints at a linkage between the two over centennial timescales. This suggests that positive feedbacks in the climate system may result in local fluctuations that are highly sensitive to small outside forcing. Finally, in Chapter 4, the attention was shifted back to the oxygen isotope record, showing that there have been a number of pronounced dry periods at the site, and these coincide with cold sea surface temperatures in the eastern Pacific, an enhanced North Pacific High, and generally dry conditions across western North America. These dry periods occur at a millennial recurrence interval, suggesting a tie with other Pacific Basin records through changes in the North Pacific Gyre system.

These studies represent initial investigation of Isabela crater lake, and the sedimentary record demonstrates variability on a range of timescales. The results suggest that going forward, a premium should be placed on combined model output and paleoproxy observations to determine mechanistic links in the climate system.

Appendix A

Stable isotope content of bulk $CaCO_3$. Composite depth is listed on left.

Core ID	Depth (cm)	Bulk $CaCO_3$ $\delta^{13}C$ (‰ VPDB)	Bulk $CaCO_3$ $\delta^{18}O$ (‰ VPDB)
MXIS 5-1	0	-11.30	-1.02
MXIS 5-1	1	-10.68	-2.46
MXIS 5-1	2	-9.19	0.06
MXIS 5-1	3	-7.52	1.31
MXIS 5-1	4	-10.18	-3.29
MXIS 5-1	5	-9.17	-1.77
MXIS 5-1	6	-7.50	0.10
MXIS 5-1	7	-7.80	-0.94
MXIS 5-1	8	-8.43	-1.73
MXIS 5-1	9	-8.61	-3.14
MXIS 5-1	10	-7.71	-1.28
MXIS 5-1	11	-8.04	-1.55
MXIS 5-1	12	-7.51	-1.84
MXIS 5-1	13	-9.87	-1.19
MXIS 5-1	14	-10.21	-1.12
MXIS 5-1	15	-9.73	-2.47
MXIS 5-1	16	-9.19	-1.32
MXIS 5-1	17	-10.80	-2.17
MXIS 5-1	18	-11.16	-1.03
MXIS 5-1	19	-11.81	-3.64
MXIS 5-1	20	-10.09	-2.29
MXIS 5-1	21	-11.26	-4.01
MXIS 5-1	22	-9.01	-3.17
MXIS 5-1	23	-10.89	-3.08
MXIS 5-1	24	-11.63	-4.03
MXIS 5-1	25	-11.43	-1.96
MXIS 5-1	26	-10.75	-2.35
MXIS 5-1	27	-12.22	-3.39
MXIS 5-1	28	-9.44	-1.53
MXIS 5-1	29	-9.73	-2.89
MXIS 5-1	30	-8.16	-1.77
MXIS 5-1	31	-8.48	-3.31
MXIS 5-1	32	-8.96	-1.28
MXIS 5-1	34	-9.28	-1.86
MXIS 5-1	35	-9.16	-2.69
MXIS 5-1	36	-10.73	-2.26
MXIS 5-1	37	-11.59	-1.58
MXIS 5-1	38	-11.91	-1.07
MXIS 5-1	39	-10.94	-1.02
MXIS 5-1	40	-10.54	-2.92
MXIS 5-1	41	-11.27	-0.94
MXIS 5-1	42	-13.17	-0.60

Core ID	Depth (cm)	Bulk $CaCO_3$ $\delta^{13}C$ (‰ VPDB)	Bulk $CaCO_3$ $\delta^{18}O$ (‰ VPDB)
MXIS 5-1	43	-13.36	-0.25
MXIS 5-1	44	-12.46	-1.39
MXIS 5-1	45	-12.12	-1.49
MXIS 5-1	46	-13.11	-0.27
MXIS 5-1	47	-13.43	0.09
MXIS 5-1	48	-14.49	-1.54
MXIS 5-1	49	-14.10	-0.46
MXIS 5-1	50	-14.58	-2.03
MXIS 5-1	51	-12.70	-1.49
MXIS 5-1	52	-12.39	-2.05
MXIS 5-1	53	-12.80	-2.60
MXIS 5-1	54	-12.44	-0.91
MXIS 5-1	55	-12.48	-1.34
MXIS 5-1	56	-12.42	-2.06
MXIS 5-1	57	-10.68	-2.05
MXIS 5-1	58	-7.68	-0.65
MXIS 5-1	59	-11.03	-0.45
MXIS 5-1	60	-6.23	-1.03
MXIS 5-1	61	-8.46	1.17
MXIS 5-1	62	-11.88	-0.62
MXIS 5-1	63	-12.91	-1.00
MXIS 5-1	64	-12.35	0.54
MXIS 5-1	65	-11.02	0.22
MXIS 5-1	66	-11.80	-0.82
MXIS 5-1	67	-13.21	-2.75
MXIS 5-1	68	-15.11	-0.91
MXIS 5-1	69	-13.12	-1.39
MXIS 5-1	70	-14.05	-0.92
MXIS 5-1	71	-14.84	-1.03
MXIS 5-1	72	-15.56	-0.64
MXIS 5-1	73	-15.08	-1.29
MXIS 5-1	74	-15.47	-0.87
MXIS 5-1	75	-13.06	-0.56
MXIS 5-1	76	-13.51	-3.31
MXIS 5-1	77	-11.21	-2.07
MXIS 5-1	78	-12.43	-0.76
MXIS 5-1	79	-12.61	-1.73
MXIS 5-1	80	-12.87	-2.73
MXIS 5-1	81	-12.73	-0.83
MXIS 5-1	82	-13.76	-1.30
MXIS 5-1	83	-12.18	-2.21
MXIS 5-1	84	-9.10	-1.35
MXIS 5-1	85	-10.32	0.48
MXIS 5-1	86	-10.44	0.07
MXIS 5-1	87	-10.97	-2.30
MXIS 5-1	88	-10.02	-1.68
MXIS 5-1	89	-10.36	-1.03

Core ID	Depth (cm)	Bulk $CaCO_3$ $\delta^{13}C$ (‰ VPDB)	Bulk $CaCO_3$ $\delta^{18}O$ (‰ VPDB)
MXIS 5-1	90	-11.03	0.80
MXIS 5-1	91	-10.83	0.75
MXIS 5-1	92	-10.92	-0.10
MXIS 5-1	93	-11.62	-0.70
MXIS 5-1	94	-13.02	-1.64
MXIS 5-1	95	-13.62	-0.99
MXIS 5-1	96	-14.86	-3.05
MXIS 5-1	97	-14.69	0.24
MXIS 5-1	98	-14.74	-0.94
MXIS 5-1	99	-14.11	-1.19
MXIS 5-1	108	-12.59	-1.05
MXIS 5-1	109	-13.82	0.24
MXIS 5-1	118	-9.52	-1.36
MXIS 5-1	119	-12.77	-0.47
MXIS 5-1	120	-12.90	-1.06
MXIS 5-1	121	-13.54	-2.41
MXIS 5-1	122	-13.11	-2.54
MXIS 5-1	124	-4.22	-0.02
MXIS 5-1	128	-11.06	-1.93
MXIS 5-1	129	-10.39	-1.89
MXIS 5-1	130	-11.78	-1.76
MXIS 5-1	131	-12.31	-2.72
MXIS 5-1	133	-2.14	-3.69
MXIS 5-1	137	-11.40	-2.62
MXIS 5-1	138	-13.44	-1.15
MXIS 5-1	139	-13.00	0.45
MXIS 5-1	140	-11.14	0.17
MXIS 5-1	141	-10.88	-0.51
MXIS 5-1	142	-11.98	-0.22
MXIS 5-1	143	-12.34	-1.80
MXIS 5-1	144	-11.95	-1.13
MXIS 5-1	145	-11.39	-0.91
MXIS 5-1	146	-8.47	-0.65
MXIS 5-1	147	-15.67	-5.74
MXIS 5-1	148	-13.18	-0.45
MXIS 5-1	149	-13.45	-0.76
MXIS 5-1	150	-14.60	-0.51
MXIS 5-1	151	-13.55	-0.55
MXIS 5-1	152	-11.90	-0.32
MXIS 5-1	153	-11.96	-1.36
MXIS 5-1	154	-14.00	-0.87
MXIS 5-1	155	-10.72	0.38
MXIS 5-1	156	-11.15	0.28
MXIS 5-1	157	-11.37	-0.71
MXIS 5-1	158	-14.51	-4.03
MXIS 5-1	159	-12.79	-1.15
MXIS 5-1	160	-11.90	-1.03

Core ID	Depth (cm)	Bulk $CaCO_3$ $\delta^{13}C$ (‰ VPDB)	Bulk $CaCO_3$ $\delta^{18}O$ (‰ VPDB)
MXIS 5-1	161	-10.86	-2.38
MXIS 5-1	162	-9.81	-1.45
MXIS 5-1	163	-11.63	-5.60
MXIS 5-1	164	-10.84	-1.41
MXIS 5-1	165	-10.43	-3.31
MXIS 5-1	166	-8.53	-1.06
MXIS 5-1	167	-7.95	1.35
MXIS 5-1	168	-8.40	-0.85
MXIS 5-1	169	-6.81	-1.98
MXIS 5-1	170	-10.94	-0.48
MXIS 5-1	171	-9.12	-1.63
MXIS 5-1	172	-11.59	-0.01
MXIS 5-1	173	-11.58	-0.25
MXIS 5-1	174	-10.51	-1.09
MXIS 5-1	175	-8.43	-0.64
MXIS 5-1	176	-6.65	0.60
MXIS 5-1	177	-9.04	0.26
MXIS 5-1	178	-7.18	0.28
MXIS 5-1	179	-10.01	0.68
MXIS 5-1	180	-12.25	-1.28
MXIS 5-1	181	-13.51	-1.38
MXIS 5-1	182	-13.59	-1.46
MXIS 5-1	183	-13.69	-1.51
MXIS 5-1	184	-8.68	0.81
MXIS 5-1	185	-14.98	-1.13
MXIS 5-1	186	-15.23	-1.32
MXIS 5-1	187	-13.97	-1.86
MXIS 5-1	188	-15.20	-1.93
MXIS 5-1	189	-13.36	-2.37
MXIS 5-1	190	-13.51	-0.63
MXIS 5-1	191	-12.31	-0.66
MXIS 5-1	192	-9.13	-1.35
MXIS 4-1	193	-9.48	-1.29
MXIS 4-1	194	-11.50	-2.83
MXIS 4-1	195	-11.01	-0.97
MXIS 4-1	196	-9.01	-1.96
MXIS 4-1	197	-7.26	-2.10
MXIS 4-1	198	-6.16	-1.34
MXIS 4-1	199	-9.71	-1.10
MXIS 4-1	200	-10.94	-1.98
MXIS 4-1	202	-11.65	-1.58
MXIS 4-1	204	-11.91	-1.12
MXIS 4-1	206	-12.71	-1.78
MXIS 4-1	208	-11.19	-1.92
MXIS 4-1	210	-11.41	-2.13
MXIS 4-1	212	-12.86	-2.13
MXIS 4-1	214	-9.01	-0.27

Core ID	Depth (cm)	Bulk $CaCO_3$ $\delta^{13}C$ (‰ VPDB)	Bulk $CaCO_3$ $\delta^{18}O$ (‰ VPDB)
MXIS 4-1	216	-12.13	-0.30
MXIS 4-1	218	-14.06	-1.90
MXIS 4-1	220	-8.44	0.05
MXIS 4-1	222	-12.94	-2.34
MXIS 4-1	224	-13.79	-2.89
MXIS 4-1	226	-10.96	-1.52
MXIS 4-1	228	-14.53	-3.22
MXIS 4-1	230	-15.31	0.34
MXIS 4-1	232	-15.34	-2.87
MXIS 4-1	234	-15.01	-1.16
MXIS 4-1	236	-15.14	-1.22
MXIS 4-1	238	-14.87	-1.39
MXIS 4-1	240	-13.27	-1.81
MXIS 4-1	242	-15.60	-1.20
MXIS 4-1	244	-13.00	-1.85
MXIS 4-1	246	-12.82	-2.38
MXIS 4-1	248	-14.28	-0.85
MXIS 4-1	250	-13.04	-0.29
MXIS 4-1	252	-12.99	-0.18
MXIS 4-1	254	-11.82	-0.33
MXIS 4-1	256	-11.72	-0.16
MXIS 4-1	258	-11.09	-0.04
MXIS 4-1	260	-12.84	-1.26
MXIS 4-1	262	-14.52	-1.58
MXIS 4-1	264	-13.92	-1.81
MXIS 4-1	266	-13.75	-2.30
MXIS 4-1	268	-12.97	-1.04
MXIS 4-1	270	-12.95	-0.47
MXIS 4-1	272	-12.85	-2.23
MXIS 4-1	274	-9.17	-1.32
MXIS 4-1	276	-8.27	-1.60
MXIS 4-1	278	-7.40	-1.78
MXIS 4-1	280	-10.99	-1.92
MXIS 4-1	282	-9.53	1.29
MXIS 4-1	284	-11.72	-0.12
MXIS 4-1	286	-11.57	-0.68
MXIS 4-1	288	-13.73	0.73
MXIS 4-1	290	-12.75	0.28
MXIS 4-1	292	-12.58	-0.39
MXIS 4-1	294	-13.04	-0.66
MXIS 4-1	296	-13.04	0.11
MXIS 4-1	298	-13.91	0.34
MXIS 4-1	300	-13.38	0.15
MXIS 4-1	302	-12.83	-0.48
MXIS 4-1	304	-13.25	0.48
MXIS 4-1	306	-13.62	-0.54
MXIS 4-1	308	-13.74	-1.41

Core ID	Depth (cm)	Bulk $CaCO_3$ $\delta^{13}C$ (‰ VPDB)	Bulk $CaCO_3$ $\delta^{18}O$ (‰ VPDB)
MXIS 4-1	310	-13.13	0.13
MXIS 4-1	312	-13.01	-0.26
MXIS 4-1	314	-12.30	-0.11
MXIS 4-1	316	-12.60	-0.04
MXIS 4-1	318	-13.00	-0.24
MXIS 4-1	320	-12.26	1.02
MXIS 4-1	321	-13.28	-0.27
MXIS 4-1	321	-13.10	-0.24
MXIS 5-2	322	-12.64	-0.24
MXIS 5-2	324	-12.90	0.07
MXIS 5-2	326	-13.21	-0.82
MXIS 5-2	328	-12.74	-0.06
MXIS 5-2	330	-12.67	0.35
MXIS 5-2	332	-11.63	0.72
MXIS 5-2	334	-13.28	0.77
MXIS 5-2	336	-13.61	1.09
MXIS 5-2	338	-12.83	0.30
MXIS 5-2	340	-11.66	0.32
MXIS 5-2	342	-10.85	0.07
MXIS 5-2	344	-12.13	0.34
MXIS 5-2	346	-12.03	-0.23
MXIS 5-2	348	-12.43	0.52
MXIS 5-2	350	-12.35	0.65
MXIS 5-2	352	-11.93	1.08
MXIS 5-2	370	-8.27	0.99
MXIS 5-2	372	-12.14	-0.52
MXIS 5-2	374	-11.57	-0.01
MXIS 5-2	376	-11.46	-1.92
MXIS 5-2	378	-4.83	2.10
MXIS 5-2	378	-9.30	0.61
MXIS 4-2	380	-5.02	0.85
MXIS 4-2	384	-4.65	1.93
MXIS 4-2	386	-9.68	-0.71
MXIS 4-2	388	-12.62	-0.85
MXIS 4-2	390	-13.67	-0.61
MXIS 4-2	392	-9.66	-1.37
MXIS 4-2	394	-7.41	-0.60
MXIS 4-2	396	-6.65	0.27
MXIS 4-2	398	-6.81	1.64
MXIS 4-2	400	-8.47	1.37
MXIS 4-2	404	-9.58	-0.30
MXIS 4-2	408	-7.31	2.42
MXIS 4-2	412	-10.45	-0.14
MXIS 4-2	416	-9.52	-2.13
MXIS 4-2	420	-9.02	0.55
MXIS 5-3	424	-7.45	-0.34
MXIS 5-3	428	-2.24	0.31

Core ID	Depth (cm)	Bulk $CaCO_3$ $\delta^{13}C$ (‰ VPDB)	Bulk $CaCO_3$ $\delta^{18}O$ (‰ VPDB)
MXIS 5-3	432	-11.44	-1.09
MXIS 5-3	436	-13.24	-0.93
MXIS 5-3	440	-7.18	-2.37
MXIS 5-3	444	-8.67	-0.94
MXIS 5-3	448	-10.26	-0.18
MXIS 5-3	452	-11.15	0.39
MXIS 5-3	456	-4.23	2.81
MXIS 5-3	460	-9.02	-1.06
MXIS 5-3	464	-11.00	-1.18
MXIS 5-3	468	-10.52	-2.77
MXIS 5-3	472	-7.63	0.38
MXIS 5-3	476	-7.36	-1.26
MXIS 5-3	480	-11.85	-2.51
MXIS 5-3	484	-10.03	0.07
MXIS 5-3	488	-9.89	-1.21
MXIS 5-3	492	-8.85	-0.20
MXIS 5-3	496	-10.00	-2.97
MXIS 5-3	499	-12.30	-1.73
MXIS 5-3	504	-8.94	-2.62
MXIS 4-2	506	-8.38	-0.02
MXIS 4-2	507	-2.25	2.18
MXIS 5-3	512	-5.35	-1.59
MXIS 5-3	516	-8.18	0.17
MXIS 5-3	520	-8.89	-1.05
MXIS 5-3	524	-9.64	-0.32
MXIS 5-3	528	-8.59	-0.10
MXIS 5-3	538	-11.39	-0.75
MXIS 4-3	542	-11.24	-1.98
MXIS 4-3	546	-9.22	-1.32
MXIS 4-3	550	-9.14	-2.00
MXIS 4-3	554	-4.48	0.17
MXIS 4-3	558	-4.77	1.30
MXIS 4-3	562	-5.04	2.09
MXIS 4-3	566	-8.89	-0.23
MXIS 4-3	570	-9.31	-0.80
MXIS 4-3	574	-9.23	-0.18
MXIS 4-3	578	-8.60	-1.99
MXIS 4-3	582	-9.72	-0.54

Core ID	Depth (cm)	Bulk $CaCO_3$	
		$\delta^{13}C$ (‰ VPDB)	$\delta^{18}O$ (‰ VPDB)
MXIS 4-3	586	-4.32	1.39
MXIS 4-3	593	-12.35	-0.26
MXIS 4-3	597	-11.86	-0.03
MXIS 4-3	601	-7.42	-1.76
MXIS 4-3	605	-7.82	-1.80
MXIS 4-3	608	-7.78	-0.77
MXIS 4-3	610	-12.43	0.01
MXIS 5-4	614	-6.96	-1.27
MXIS 5-4	618	-8.29	-0.31
MXIS 5-4	622	-9.80	-2.33
MXIS 5-4	626	-13.13	-1.85
MXIS 5-4	630	-12.63	-1.07
MXIS 5-4	634	-9.87	-0.51
MXIS 5-4	636	2.49	3.05
MXIS 4-3	640	-10.02	-0.27
MXIS 4-3	644	-10.45	-0.63
MXIS 4-3	648	-6.43	0.81
MXIS 4-3	652	-10.26	-0.53
MXIS 4-3	656	-10.59	-0.32
MXIS 4-3	660	-10.44	-2.80
MXIS 4-3	664	-9.36	-1.10
MXIS 4-3	668	-8.50	-0.80
MXIS 4-3	672	-3.84	0.50
MXIS 4-3	676	-11.16	-1.23
MXIS 4-3	680	-11.40	-0.99
MXIS 4-3	684	-2.84	0.99
MXIS 4-3	688	-10.91	-0.69
MXIS 4-3	692	-9.03	0.22
MXIS 4-3	696	-9.58	-0.13
MXIS 4-3	700	-7.74	-0.92
MXIS 4-3	704	-6.49	0.20
MXIS 4-3	708	-8.93	0.55
MXIS 4-3	712	-4.16	1.87
MXIS 4-3	714	-10.15	1.07
MXIS 5-4	718	-9.80	-0.36
MXIS 5-4	722	-9.79	-0.13
MXIS 5-4	726	-10.62	-0.10
MXIS 5-4	730	-10.94	-0.54
MXIS 5-4	734	-5.13	1.39
MXIS 5-4	738	-11.70	-0.50
MXIS 5-4	742	-8.82	-1.40
MXIS 5-4	746	-3.30	1.59
MXIS 5-4	750	-12.20	-1.65
MXIS 5-4	754	-4.06	0.80
MXIS 5-4	758	-8.73	-0.01
MXIS 5-4	760	-8.31	-0.36

Core ID	Depth (cm)	Bulk $CaCO_3$ $\delta^{13}C$ (‰ VPDB)	Bulk $CaCO_3$ $\delta^{18}O$ (‰ VPDB)
MXIS 4-4	764	-0.66	2.35
MXIS 4-4	768	-5.73	0.57
MXIS 4-4	772	-7.02	0.48
MXIS 4-4	776	-8.17	-0.67
MXIS 4-4	780	-8.91	-0.93
MXIS 4-4	784	-6.33	-1.70
MXIS 4-4	788	-7.54	-0.73
MXIS 4-4	792	-7.52	-2.56
MXIS 4-4	796	-4.02	-0.08
MXIS 4-4	800	-9.03	-2.28
MXIS 4-4	804	-8.33	-0.23
MXIS 5-5	808	-5.67	-0.55
MXIS 5-5	812	-7.19	-0.86
MXIS 5-5	816	-0.45	2.39
MXIS 5-5	844	-8.84	-3.70
MXIS 5-5	848	-3.13	-0.56
MXIS 5-5	860	-6.99	1.18
MXIS 5-5	868	-5.49	0.98
MXIS 5-5	872	-7.51	-1.90
MXIS 5-5	876	-4.42	2.73
MXIS 5-5	884	-7.17	-3.62
MXIS 5-5	888	-11.62	-1.45
MXIS 5-5	891	-5.54	0.66
MXIS 5-5	896	-10.31	-3.03
MXIS 5-5	900	-6.11	0.80
MXIS 5-5	904	-4.95	0.21
MXIS 5-5	908	-9.29	-3.35
MXIS 5-5	912	-3.91	0.44
MXIS 5-5	916	-7.91	1.52
MXIS 5-5	920	-5.67	0.36
MXIS 5-5	924	-3.75	0.94
MXIS 5-5	928	-5.35	2.96
MXIS 5-5	932	-8.72	0.34
MXIS 5-5	936	-3.88	0.01
MXIS 5-5	940	-1.36	-0.92
MXIS 5-5	944	-8.49	0.52
MXIS 5-5	948	-7.08	0.33
MXIS 5-5	952	-7.17	-2.17
MXIS 5-5	956	-5.80	1.04
MXIS 5-5	960	-5.46	0.06
MXIS 5-5	964	-5.91	-0.95
MXIS 5-5	968	-2.01	0.22
MXIS 5-5	972	-9.35	-1.00
MXIS 5-5	976	-5.29	1.86
MXIS 5-5	980	-3.43	0.90
MXIS 5-5	984	-6.23	-1.16
MXIS 5-5	988	-1.99	2.98

Core ID	Depth (cm)	Bulk $CaCO_3$ $\delta^{13}C$ (‰ VPDB)	Bulk $CaCO_3$ $\delta^{18}O$ (‰ VPDB)
MXIS 5-5	990	-7.61	-0.25
MXIS 6-1	998	-6.92	-0.65
MXIS 6-1	1002	-8.42	-0.72
MXIS 6-1	1006	-5.99	-0.64
MXIS 6-1	1010	-5.81	-0.11
MXIS 6-1	1014	-6.03	-0.58
MXIS 6-1	1018	-6.19	-0.61
MXIS 6-1	1022	5.40	4.80
MXIS 6-1	1026	-8.18	0.60
MXIS 6-1	1030	-9.83	-0.09
MXIS 6-1	1034	-1.81	0.71
MXIS 6-1	1038	-5.15	2.23
MXIS 6-1	1042	-5.45	0.66
MXIS 6-1	1046	-6.39	1.21
MXIS 6-1	1050	-4.90	0.91
MXIS 6-1	1054	-8.36	0.48
MXIS 6-1	1058	-10.06	2.54
MXIS 6-1	1062	-8.05	1.20
MXIS 6-1	1066	-9.34	1.07
MXIS 6-1	1070	-7.97	1.85
MXIS 6-1	1074	-5.70	1.15
MXIS 5-6	1078	-6.86	0.77
MXIS 5-6	1082	-6.79	0.55
MXIS 5-6	1086	-3.64	1.10
MXIS 5-6	1090	-7.18	1.33
MXIS 5-6	1094	-7.42	1.35
MXIS 5-6	1098	-9.36	-0.84
MXIS 6-1	1102	-5.66	1.70
MXIS 6-1	1106	-4.79	0.74
MXIS 6-1	1110	-4.99	1.71
MXIS 6-1	1111	-2.24	2.08
MXIS 5-6	1118	-4.48	0.93
MXIS 5-6	1122	-3.54	1.32
MXIS 5-6	1126	-4.84	0.97
MXIS 5-6	1130	-4.32	0.93
MXIS 5-6	1134	-5.20	0.52
MXIS 5-6	1138	-6.88	0.19
MXIS 5-6	1142	-5.99	0.25
MXIS 5-6	1146	-5.90	0.31
MXIS 5-6	1150	-6.12	0.39
MXIS 5-6	1154	-7.27	0.34
MXIS 5-6	1158	-6.90	0.35
MXIS 5-6	1162	-6.95	0.64
MXIS 5-6	1166	-7.36	0.19
MXIS 5-6	1170	-7.47	0.63
MXIS 5-6	1186	-5.41	0.78
MXIS 5-6	1190	-6.01	1.85

Core ID	Depth (cm)	Bulk $CaCO_3$ $\delta^{13}C$ (‰ VPDB)	Bulk $CaCO_3$ $\delta^{18}O$ (‰ VPDB)
MXIS 5-6	1192	-6.25	0.65
MXIS 6-2	1196	-7.09	1.06
MXIS 6-2	1200	-6.19	0.99
MXIS 6-2	1204	-6.63	0.94
MXIS 6-2	1208	-7.89	1.12
MXIS 6-2	1212	-6.83	1.36
MXIS 6-2	1216	-6.26	0.85
MXIS 6-2	1220	-5.21	0.83
MXIS 6-2	1224	-5.89	0.89
MXIS 6-2	1228	-5.84	0.71
MXIS 6-2	1232	-4.02	0.72
MXIS 6-2	1236	-4.84	0.82
MXIS 6-2	1240	-2.11	1.09
MXIS 6-2	1244	-2.61	1.56
MXIS 6-2	1248	-2.76	1.88
MXIS 6-2	1252	-7.00	0.37
MXIS 6-2	1256	-5.58	0.78
MXIS 6-2	1260	-5.59	0.86
MXIS 6-2	1264	-6.12	0.27
MXIS 6-2	1268	-0.54	1.55
MXIS 6-2	1276	2.90	3.70
MXIS 4-5	1280	5.63	3.97
MXIS 4-5	1284	4.23	3.59
MXIS 4-5	1288	4.38	2.49
MXIS 4-5	1292	5.89	4.35
MXIS 4-5	1300	-2.44	1.54
MXIS 4-5	1304	-1.60	1.46
MXIS 4-5	1308	-3.62	0.05
MXIS 4-5	1312	-3.75	0.28
MXIS 6-2	1316	-2.54	0.98
MXIS 6-2	1320	0.31	1.84
MXIS 6-2	1324	-4.57	-0.33
MXIS 6-2	1328	-5.06	0.21
MXIS 6-2	1332	-2.64	0.01
MXIS 6-2	1336	-1.03	0.59
MXIS 6-2	1344	-5.34	-0.20
MXIS 6-2	1348	-0.39	1.43
MXIS 6-2	1352	2.21	1.29
MXIS 6-2	1360	-2.56	-0.03
MXIS 6-2	1364	-3.20	0.13
MXIS 6-2	1372	-1.85	1.49
MXIS 6-2	1376	-3.63	1.15
MXIS 6-2	1380	-3.68	-0.92
MXIS 6-2	1384	-2.49	0.29
MXIS 6-2	1391	2.76	0.06

Appendix B

The age model for the record was constructed using eight calendar-corrected radiocarbon ages. A tephra layer located at 1.6 cm sediment depth corresponds to the 1998-1999 eruption of the Colima volcano, confirming that the top core sections accurately captured the sediment-water interface.

The radiocarbon ages were determined using ~1 mg samples of bulk acid insoluble organic matter. Sediment samples were acidified at 90°C using 1N HCl, rinsed with distilled water to neutral pH, and dried overnight. Following combustion to CO_2, samples were reduced to graphite using iron as a catalyst, after Vogel et al. (1984). A standard coal blank was treated simultaneously with the samples and used for background subtraction. Radiocarbon content was measured at the Center for Accelerator Mass Spectrometry (CAMS), at Lawrence Livermore National Laboratory. Radiocarbon ages are reported using the Libby half-life of 5568 yr, following standard conventions (Stuiver and Polach, 1977), and includes a $d^{13}C$ correction of -23‰.

An age of 360±35 ^{14}C yr BP was obtained from surface sediments, indicating that there is a source of pre-aged carbon in the lake or catchment. This age represents a weighted average of organic matter inputs to the lake, and reflects both the regional marine carbon reservoir effect (from seabird guano input to the lake; 910±60 ^{14}C yr BP, Ingram and Southon, 1996), primary productivity and recycling of organic matter within the water column, and terrestrial inputs from the catchment. The ΔR of 360 ^{14}C yr BP was assumed to be constant over this core section, and calibrated ages were determined using CALIB 6.0 (Reimer et al., 2009). The ARAND software program was used to interpolate between calibrated radiocarbon ages (Howell, et al., 2006).

Table B1. Radiocarbon chronology.

CAMS #	Depth (cm)	fraction Modern	±	$\Delta^{14}C$	±	^{14}C Age (^{14}C yr BP)	±
136255	12	0.9563	0.0036	-50.4	3.6	360	35
136256	15	0.9519	0.0036	-54.7	3.6	395	35
137056	19	0.9471	0.0038	-59.5	3.8	435	35
136258	42	0.9367	0.0044	-69.8	4.4	525	40
136259	55	0.9371	0.0042	-69.5	4.2	520	40
136260	65	0.9291	0.0035	-77.4	3.5	590	35
140535	78	0.9305	0.0036	-69.5	3.6	580	35
140536	178	0.8715	0.0034	-128.5	3.4	1105	35

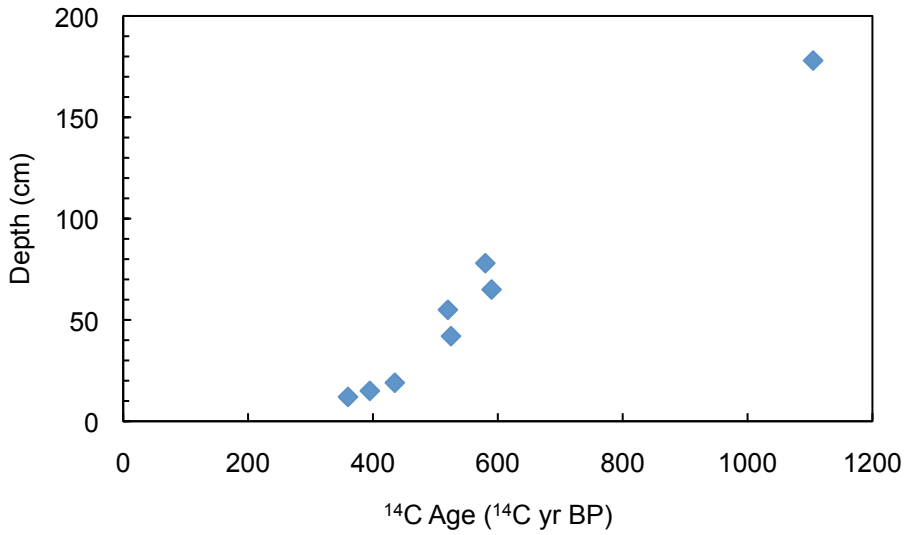


Figure B1. Age-depth relationship in Isabela crater lake sediments.